

# FT-IR Photoacoustic Spectroscopy

John F. McClelland<sup>1,2</sup>, Roger W. Jones<sup>2</sup>, and Stanley J. Bajic<sup>2</sup>

<sup>1</sup>MTEC Photoacoustics, Inc.  
PO Box 1095  
Ames, IA 50014  
[www.mtecpas.com](http://www.mtecpas.com)  
515-292-7974  
FAX: 515-292-7125  
mcclelland@mtecpas.com

<sup>2</sup>Ames Laboratory – US DOE  
107 Spedding Hall  
Iowa State University  
Ames, IA 50011-3020 USA

February, 2002

This is a print of a chapter that appears in  
*Handbook of Vibrational Spectroscopy*  
edited by John M. Chalmers and Peter R. Griffiths  
and published by John Wiley & Sons, Ltd.

## Introduction

The desired result with all Fourier transform infrared (FT-IR) sampling techniques is to obtain an absorbance spectrum of the sample as quickly and easily as possible. In many cases, however, direct analysis of “as received” samples by transmission or reflection methods is not practical because the sample either transmits inadequate light to measure or it lacks suitable surface or particle size conditions for reflectance spectroscopies. In other cases, reflectance spectroscopies may not probe deeply enough into the sample to yield the desired information.

Photoacoustic spectroscopy (PAS)<sup>1-3</sup> is unique as a sampling technique, because it does not require that the sample be transmitting, has low sensitivity to surface condition, and can probe over a range of selectable sampling depths from several micrometers to more than 100  $\mu\text{m}$ . PAS has these capabilities because it directly measures infrared (IR) absorption by sensing absorption-induced heating of the sample within an experimentally controllable sampling depth below the sample’s surface. Heat deposited within this depth transfers to the surrounding gas at the sample surface, producing a thermal-expansion-driven pressurization in the gas, known as the PAS signal, which is detected by a microphone. The magnitude of the PAS signal varies linearly with increasing absorptivity, concentration or sampling depth until at high values of their product a gradual roll off in sensitivity (saturation) occurs. The phase of the PAS signal corresponds to the time delay associated with heat transfer within the sample. These signal components are described in detail in the next section.

PAS signal generation is initiated when the FT-IR beam, which oscillates in intensity, is absorbed by the sample resulting in the absorption-induced heating in the sample and oscillation of the sample temperature. The temperature oscillations occurring in each light-absorbing layer within the sample launch propagating temperature waves called thermal-waves, which decay strongly as they propagate through the sample. It is this thermal-wave decay process that defines the layer thickness, or sampling depth, from which spectral information is obtained in an FT-IR PAS analysis. The sampling depth can be increased by decreasing, via FT-IR computer control, the IR beam modulation frequency imposed by the interferometer. The lower modulation frequency allows a longer time for thermal-waves to propagate from deeper within the sample into the gas. As the sampling depth increases, the saturation of strong bands in PAS spectra increases just as it does in absorption spectra measured by transmission as sample thickness increases.

The discovery of the photoacoustic effect by Alexander Graham Bell in 1880 marked the beginning of the development of the technique as a useful spectroscopic method.<sup>4</sup> Development was hampered, however, by the weak acoustic signals that must be measured due to the very high thermal-wave reflection coefficient at the sample-to-gas interface. A high fraction of the thermal-wave amplitude is reflected back into the sample and is not detected, leading to signal-to-noise problems. Signal saturation also was a problem in the initial efforts to apply the technique in the ultraviolet and visible spectral regions. Operation in the near- and mid-infrared spectral regions, made practical

with the multiplexing capability of FT-IR systems and the higher sensitivity of photoacoustic detectors, has been a major area of success for the PAS technique. These spectral regions are rich in chemical information, and modern search and chemometric software allow qualitative and quantitative results to be readily obtained from PAS spectra in the presence of the more modest saturation effects found in these spectral regions. At this time, FT-IR PAS is a broad field of research that continues to develop in the areas of instrumentation, applications, and data analysis. This article will be restricted to primarily FT-IR PAS of solid samples and to a much lesser degree of liquids.

The article **Transient Infrared Spectroscopy** for on-line analyses may also be of interest to readers because transient infrared spectroscopy (TIRS) is also a thermal-wave based technique that has similar capabilities to PAS but operates on moving samples.

### Photoacoustic Signal Generation, Processing and Interpretation

The photoacoustic signal contains information on the sample's absorption spectrum and on the depth below the sample's surface from which the signal evolves, allowing materials with layered or gradient compositions to be studied. Photoacoustic signal generation can be modeled<sup>5,6</sup> using the heat equation<sup>7</sup> and assuming a one-dimensional heat flow within the sample and adjacent gas atmosphere that is in the direction opposite to that of the light beam. The most instructive model for general purposes also assumes an optically and thermally homogeneous slab sample geometry which is thick on the scale of the thermal-wave decay length with the rear sample face thermally grounded and optically nonreflective. The model is shown schematically in Figure 1.

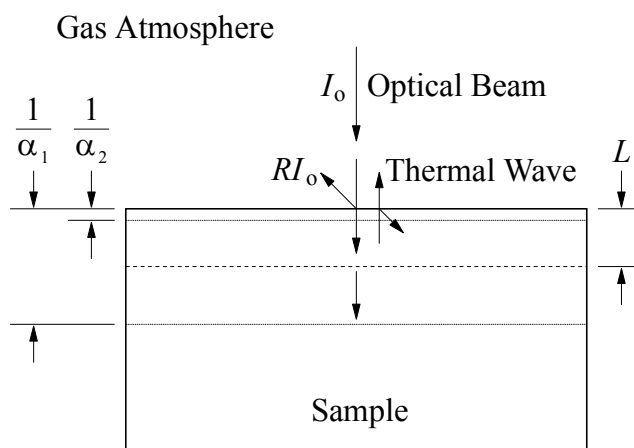


Figure 1. One-dimensional signal generation schematic showing the decay length,  $L$ , for thermal-waves and the optical decay lengths for lower ( $\alpha_1$ ) and higher ( $\alpha_2$ ) values of absorption coefficient. As  $\alpha$  increases, more of the absorption occurs in the region near the sample's surface that is active in signal generation. Reproduced from Reference 3.

The FT-IR interferometer modulates the intensity of the infrared beam that is incident on the sample. The beam is partially reflected ( $RI_0$ ) at the front face of the sample but this reflection is ignored in the simple model. The beam then decays exponentially with an absorption coefficient,  $\alpha(\tilde{\nu})$ , as it propagates within the sample.

The wavenumber of the infrared radiation is denoted by  $\tilde{\nu}$ . In most cases all of the absorbed radiation is converted into heat, causing the temperature of each absorbing layer to oscillate at the beam modulation frequency with an amplitude proportional to the amount of light absorbed in it. Each of these layers becomes a source for launching propagating temperature oscillations called thermal waves.

Thermal waves have three important properties affecting photoacoustic signal generation. They have a short decay length called the thermal diffusion depth or thermal wave decay length,  $L$ , given by equation (1):

$$L = (D/\pi f)^{1/2} \quad (1)$$

where  $D$  and  $f$  denote the sample's thermal diffusivity and the infrared beam modulation frequency, respectively. Thermal waves decay to 37% (i.e.  $1/e$ ) of their original amplitude over a distance of  $L$ . If the decay of thermal waves did not define an active signal-generation layer that is smaller than the optical decay length, photoacoustic spectra of opaque samples would be just as hopelessly saturated and impractical for measurement as transmission spectra are for such samples. Fortunately, as long as the thin layer is partially transmitting, the photoacoustic signal increases with absorption coefficient and spectra can be readily measured by PAS, regardless of sample thickness.

After the thermal waves are launched, those that propagate to the front face of the sample contribute to the PAS signal, but most of their amplitude is not detected because it is reflected back into the sample and decays. The strong back reflection of thermal waves in the solid is the second important property of thermal waves in photoacoustic signal generation, but it is not as fortuitous for the signal generation process as is their short decay length. In fact, if the high back reflection were not present, photoacoustic signals would have significantly higher amplitudes and signal-to-noise ratios.

The small thermal-wave amplitude that does transmit into the gas results in thermal expansion and a pressure oscillation in the gas, which increases with  $\alpha(\tilde{\nu})$  and that is detected as an acoustic signal containing both phase and magnitude information by a sensitive microphone. The phase of the PAS signal is equal to the phase lag between the signal and the waveform of the IR beam that excites it. The lag is caused by the finite propagation time of thermal waves during signal generation. This is the third important property of thermal waves in signal generation and it results in the phase angle being a measure of the depth from which the signal evolves within the sample. The maximum phase angle that can be measured is one cycle, or  $360^\circ$ , corresponding to a maximum depth of  $2\pi L$  on the length scale.

In many instances, PAS data are analyzed in the form of magnitude spectra. These spectra are commonly used for qualitative and quantitative analysis of

homogeneous samples. Nonhomogeneous samples that have been either homogenized by size reduction or sampled multiple times to assure good sampling statistics, are also suitable for analysis using magnitude spectra. Magnitude spectra measured at different modulation frequencies are used to study samples having compositional variations as a function of depth often in combination with phase spectra.

PAS signal dependence on  $\alpha$  is nonlinear at the extremes of low and high values of  $\alpha$ . The PAS magnitude signal experiences a background signal “floor” at very low values of  $\alpha$  (typically less than  $1 \text{ cm}^{-1}$ ), due to the absorption of light by contamination on the sample chamber walls and on the sample itself, and to an acoustic-piston<sup>6</sup> sample response. Above this floor, the signal goes through a linear range with increasing  $\alpha$  as predicted by the simple model until at a value of  $\alpha$ , denoted by  $\alpha_o$  the signal experiences an onset of signal saturation and starts to lose sensitivity to increasing values of  $\alpha$ . Full saturation occurs at a higher value of  $\alpha$ , denoted by  $\alpha_f$ , where the PAS signal no longer senses increases in absorption coefficient. Table 1 gives the absorption coefficient values for different modulation frequencies estimated from the simple model for the onset and full saturation conditions, assuming a homogeneous sample. Note that as the modulation frequency increases,  $\alpha_o$  and  $\alpha_f$  shift to higher absorption coefficient values due to a thinning of the active layer generating the signal. Another important point is that the absorption coefficient continues to increase for over two orders of magnitude above the onset of saturation before the signal loses all sensitivity to  $\alpha$  at  $\alpha_f$ . The simple model can be used to make useful connections between the sample’s optical and thermal properties resulting in approximate rule of thumb values for  $\alpha_o$ ,  $\alpha_f$ , and  $\alpha_{ll}$  as a function of  $L$ :

$$\alpha_o \cong 1/10L \quad (2)$$

$$\alpha_f \cong 20/L \quad (3)$$

$$\alpha_{ll} \cong 100/L \quad (4)$$

$\alpha_{ll}$  of Equation 4 is referred to as the linearization limit and it marks the practical upper limit that can be reached when photoacoustic magnitude and phase data are combined to calculate so-called linearized magnitude spectra.<sup>3,8-10</sup> Linearized PAS spectra vary linearly with  $\alpha$  to approximately three orders of magnitude above the onset of saturation observed for purely magnitude spectra. The linearization process involves measuring single beam spectra for the sample and for a glassy carbon reference, shifting the interferograms, if necessary, so that they have the same centerburst retardations, and transforming the interferograms using the same phase correction to obtain the real (R) and imaginary (I) components. The linearized spectrum,  $S_l$ , is then calculated from<sup>10</sup>

$$S_l = (S_R^2 + S_I^2)/1.414 (S_I R_R - S_R R_I) \quad (5)$$

where the subscripts R and I denote the real and imaginary components of the sample (S) and reference (R) spectra. Explicit  $\tilde{\nu}$  dependence has been omitted in Equation (5).

Table 1. Rule of thumb absorption coefficient values ( $\text{cm}^{-1}$ ) derived from the simple model that characterizes PAS signal generation in polymers assuming  $D = 10^{-3} \text{ cm}^2/\text{s}$ .

	<u>10 Hz</u>	<u>100 Hz</u>	<u>1000 Hz</u>	<u>10,000 Hz</u>
$\alpha_o$ (onset of saturation)	18	56	180	560
$\alpha_f$ (full saturation)	3300	$1.1 \cdot 10^4$	$3.3 \cdot 10^4$	$1.1 \cdot 10^5$
$\alpha_{ll}$ (linearization limit)	$2 \cdot 10^4$	$6.3 \cdot 10^4$	$2 \cdot 10^5$	$6.3 \cdot 10^5$

Linearization of magnitude spectra has two primary advantages. The most important is that the sampling depth in effect is reduced by approximately a factor of 3 going from pure magnitude to linearized magnitude spectra. This results in the emphasis of spectral features due to thin surface layers with higher surface specificity than can be obtained from a purely magnitude spectrum taken at the highest FT-IR mirror velocity available.

The second advantage is, of course, the reduction or removal of saturation in strong absorbance bands, which may be valuable in quantitative analyses. In many cases, however, chemometric programs tolerate significant amounts of saturation in spectra very well and produce excellent quantitative data, making linearization unnecessary for this purpose.

Another issue related to signal saturation occurs when sampling depth is varied to investigate samples of depth-varying composition. As the modulation frequency is increased to produce shallower sampling, the magnitude of spectral bands change for two reasons: (i) bands associated with species concentrated closer to the surface increase relative to bulk bands and vice versa; and (ii) bands that are saturated also increase relative to weaker bands due to reduction in the level of saturation since, in effect, a thinner sample is being analyzed. These two effects are easily observed if the two spectra, taken at different modulation frequencies, are scaled so that a weak matrix band, which has no saturation in either spectrum, is of constant amplitude. This has customarily been the practice in order to put the spectra on as common a scale as possible, but it leaves the problem of the separation of band changes due to composition versus saturation unresolved.

The simple signal-generation model, however, provides a basis for converting a low-modulation-frequency spectrum into a spectrum with nearly the same degree of saturation as a higher-frequency spectrum. This PAS saturation compensation approach essentially removes the saturation differences while retaining any differences related to sample structure. The method uses only magnitude spectra and requires no phase information.

The conversion process is as follows. For a thermally thick sample with a negligible thermal expansion signal contribution and ignoring reflectance, Equation (41) of McDonald and Wetsel<sup>6</sup> gives the photoacoustic signal,  $S(\tilde{\nu})$ , as equation (6):

$$S(\tilde{\nu}) = \frac{j}{2\pi f} \frac{\gamma P_0}{l_g} \frac{I_0}{2\rho_s C_{ps}} \frac{\alpha(\tilde{\nu})}{\sigma_g T_0 (g+1)(r+1)} \quad (6)$$

where  $j = (-1)^{1/2}$ ,  $f$  is the modulation frequency,  $I_0$  is the incident light intensity,  $T_0$  and  $P_0$  are the ambient temperature and pressure,  $l_g$  and  $\gamma$  are the thickness and heat-capacity ratio of the gas,  $\alpha(\tilde{\nu})$  is the absorption coefficient of the sample,  $\rho_s$  and  $C_{ps}$  are the density and heat capacity of the sample,  $g = (\kappa_g \sigma_g) / (\kappa_s \sigma_s)$ ,  $\sigma_g = (j2\pi f / D_g)^{1/2}$ ,  $\sigma_s = (j2\pi f / D_s)^{1/2}$ ,  $D_g$  and  $D_s$  are the thermal diffusivities of the gas and sample,  $\kappa_g$  and  $\kappa_s$  are the thermal conductivities of the gas and sample, and  $r = \alpha(\tilde{\nu}) / \sigma_s$ . For two spectra taken at modulation frequencies  $f$  and  $Nf$ , the ratio of their magnitudes after normalization,  $Q(\tilde{\nu})$ , can be derived from Equation (7):

$$Q(\tilde{\nu}) = N \frac{S_{Nf}(\tilde{\nu})}{S_f(\tilde{\nu})} = \frac{r+1}{r+N^{1/2}} \quad (7)$$

where  $r$  is evaluated at frequency  $f$ , and it is assumed that the reference used for normalization has the  $1/f$  frequency dependence typical of a strong absorber. Of course, in nonphase-modulation FT-IR PAS the modulation frequency is not constant within a spectrum, but depends on wavenumber. Nevertheless, Equation (7) still applies because the modulation frequencies of the two spectra differ by  $N$  at each wavenumber when the scanning speeds of the two spectra differ by  $N$ . Multiplying a spectrum at one scanning speed by  $Q(\tilde{\nu})$  would convert it into a spectrum at  $N$  times the scanning speed, but because  $r$  is a sample-dependent quantity, Equation (7) by itself cannot be applied without knowing the physical properties of the sample. To produce a universal, sample-independent equation,  $r$  must be eliminated. This can be done by putting the low-frequency spectrum on a scale where the maximum possible signal is one. This scaled magnitude,  $S_{sc}(\tilde{\nu})$ , can be derived from Equation (8):

$$S_{sc}(\tilde{\nu}) = \frac{S_f(\tilde{\nu})}{\lim_{\alpha \rightarrow \infty} S_f(\tilde{\nu})} = \frac{r}{r+1} \quad (8)$$

Combining Equations (7) and (8) allows  $Q(\tilde{\nu})$  and  $S_{sc}(\tilde{\nu})$  to be given in terms of one another, independent of sample-specific quantities as shown in equations (9) and (10):

$$Q(\tilde{\nu}) = \frac{1}{N^{1/2}(1 - S_{sc}(\tilde{\nu})) + S_{sc}(\tilde{\nu})} \quad (9)$$

$$S_{sc}(\tilde{\nu}) = \frac{N^{1/2}Q(\tilde{\nu}) - 1}{Q(\tilde{\nu})(N^{1/2} - 1)} \quad (10)$$

Figure 2 shows the relationship between  $Q(\tilde{\nu})$  and  $S_{sc}(\tilde{\nu})$  for selected frequency ratios.

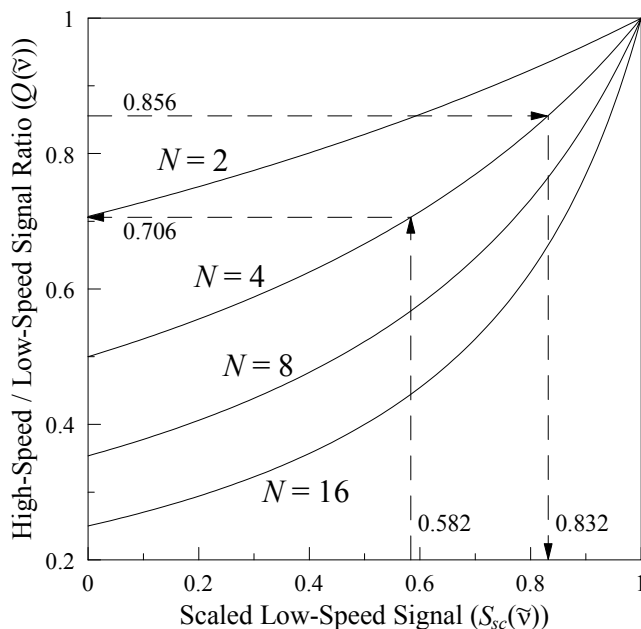


Figure 2. The ratio of the magnitudes of two normalized spectra whose scanning speeds differ by a ratio,  $N$ , as a function of the magnitude of the low-speed spectrum scaled to a maximum of 1.

How are Equations (9) and (10) used to convert a low-scanning-speed spectrum into a high-scanning-speed equivalent? First, spectra at the two scanning speeds are acquired, such as the spectra in Figure 3 for a poly(methyl methacrylate) (PMMA) disk. The dashed-line spectrum was acquired at 0.158 cm/s (retardation change velocity) and the solid-line spectrum was acquired at 0.632 cm/s, so they differ by a speed ratio of 4;  $N = 4$ . Next, one peak in the spectra is chosen as a guide. This peak must arise solely from a homogeneously distributed component in a gradient sample or be a strong absorption in the first (outer layer of a layered sample) so that it follows the homogeneous-sample behavior of the theory. Also, it is best if the peak is neither very weak, which could decrease the accuracy of the conversion, nor very strong, which could be approaching full saturation. The value of  $Q(\tilde{\nu})$  for that peak is determined from the peak's heights in the two spectra, and then  $S_{sc}(\tilde{\nu})$  for the peak is calculated from  $Q(\tilde{\nu})$  using Equation (10). The peak at  $1153 \text{ cm}^{-1}$  can be the guide for the Figure 3 spectra; it has a  $Q(\tilde{\nu})$  value of 0.856. As Figure 2 illustrates, a value of 0.856 for  $Q(\tilde{\nu})$  means  $S_{sc}(\tilde{\nu})$  is 0.832 when  $N$  is four. The  $S_{sc}(\tilde{\nu})$  value for the guide peak fixes the  $S_{sc}(\tilde{\nu})$  scale for every point in the low-speed spectrum. For example, the  $1450 \text{ cm}^{-1}$  peak in Figure 3 is seven-tenths the size of the guide peak (in the low-speed



spectrum). That means its  $S_{sc}(\tilde{\nu})$  value is  $0.70(0.832) = 0.582$ . This scaling is done for the whole low-speed spectrum so that the  $S_{sc}(\tilde{\nu})$  value for every data point in the spectrum is known. Equation (9) is then used to determine what  $Q(\tilde{\nu})$  should be for every point in the spectrum. Multiplying each point in the low-speed spectrum by its value for  $Q(\tilde{\nu})$  converts the low-speed spectrum into the high-speed-spectrum equivalent. For the example peak at  $1450\text{ cm}^{-1}$ , Figure 2 shows that its  $S_{sc}(\tilde{\nu})$  value of 0.582 corresponds to  $Q(\tilde{\nu}) = 0.706$ , so in the conversion of the low-speed spectrum to the high-speed equivalent, the data point at the peak of the  $1450\text{ cm}^{-1}$  band is multiplied by 0.706. When this is done for every point in the low-speed spectrum, the spectrum shown by the dotted line in Figure 3 results. Because the PMMA sample is homogeneous and thermally thick, the converted spectrum should be identical to the true high-speed spectrum. They are very similar, if not quite identical. The difference between the two is shown by the heavy solid line near zero in Figure 3. This residual spectrum is not exactly zero because the simple-model theory of Equation (6) neglects various second-order effects. The most prominent error is the derivative-like shape of the residual spectrum at many peak locations. This comes from the characteristic change in sample reflectivity near absorption peaks, which is not included in the theory.

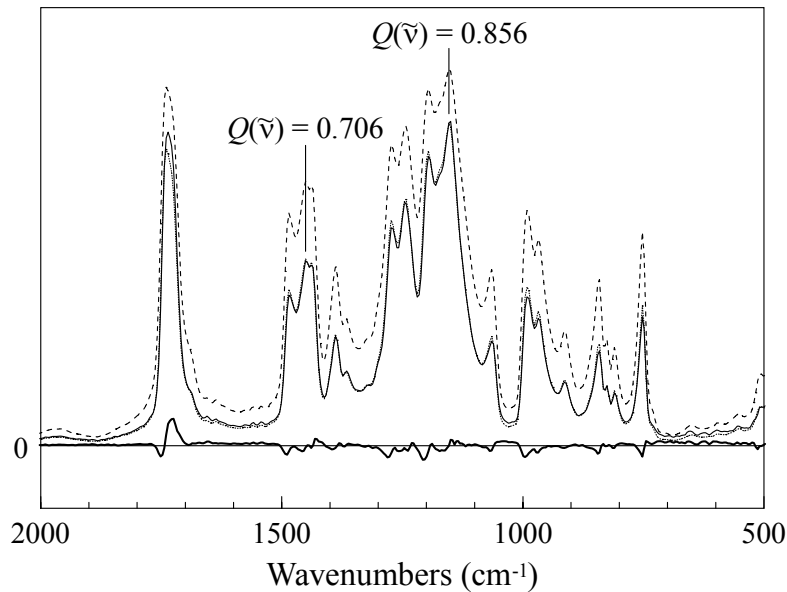


Figure 3. Photoacoustic magnitude spectra for a homogeneous PMMA sample, where the dashed line is the low frequency spectrum before saturation compensation and the dotted curve is after compensation. The lower trace is the high frequency spectrum minus the compensated spectrum, where the high frequency spectrum is the upper solid trace.

Even though the match between converted and true high-speed spectra is not perfect, the approach removes most of the effects of the speed change for bands coming from homogeneous components, so it can be very useful in depth investigations. Figure 4 demonstrates this on a polypropylene sample containing a gradient additive whose concentration diminishes with depth within the sample. The dashed and solid lines are 0.00316 and 0.0506 cm/s spectra of the sample, so  $N = 16$ , and the dotted line is the low-speed spectrum converted to a 0.0506 cm/s equivalent, using the  $1458\text{ cm}^{-1}$  band as the guide peak. The  $1458\text{ cm}^{-1}$  peak was chosen as the guide because it comes solely from the polypropylene matrix (i.e., a homogeneous component). The thick solid line is the difference between the true and converted 0.0506 cm/s spectra. The short, vertical lines on the zero-level grid line mark the locations of the 17 strongest absorption bands of the additive. Almost all of these are present in the difference spectrum, and they account for the major features in the difference spectrum.

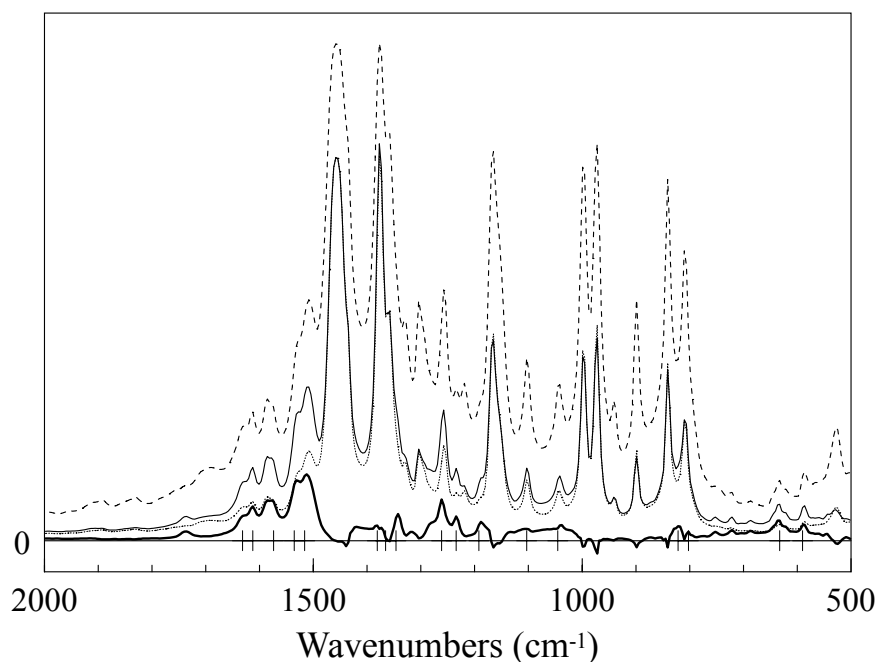


Figure 4. Photoacoustic magnitude spectra for a polypropylene sample with an additive gradient that increases with depth. The dashed line is the low frequency spectrum before saturation compensation and the dotted after. The solid traces are the high frequency spectrum (upper) and difference spectrum (lower) that reveals the additive. See text for more details.

The capability of varying sampling depth is a key feature of PAS.  $L$  has often been referred to as the sampling depth of PAS, but in reality it sets a depth scale rather than a certain depth. The actual sampling depth limit in FT-IR PAS is the distance that a

thermal wave can travel in the time period,  $T = 1/f$ , of the IR beam modulation. Thermal waves travel with a velocity  $(4\pi f D)^{1/2}$ ,<sup>7</sup> resulting in a propagation distance in the time  $T$  of  $2\pi L$ . Over this distance the thermal wave amplitude decays by a factor of  $1.87 \cdot 10^{-3}$  so it is not always practical to measure magnitude and phase signals from this depth due to signal-to-noise and background signal considerations.

It is also important to note that the decay of thermal waves is not the determining factor in spectral regions of very high absorption. If light is not transmitted as deep as  $2\pi L$ , then the decay of light - rather than decay of thermal waves - is dominant in determining the sampling depth. Figure 5 demonstrates a case where sampling depth, and therefore the degree of saturation, is determined by optical absorption rather than by thermal wave decay. The spectra in Figure 5 were measured on oil samples with  $L$  held constant and the absorption controlled by adding carbon black to the liquid sample. The spectra were shifted so that they have a common zero baseline at  $2700 \text{ cm}^{-1}$  and were scaled with equal amplitude for a point in the spectrum ( $2820 \text{ cm}^{-1}$ ), which is little affected by saturation relative to the high saturation of the absorption peaks. This scaling allows the decrease in spectral saturation to be observed that occurs as the sampling depth is decreased by the shorter optical path length caused when the carbon black concentration is increased.

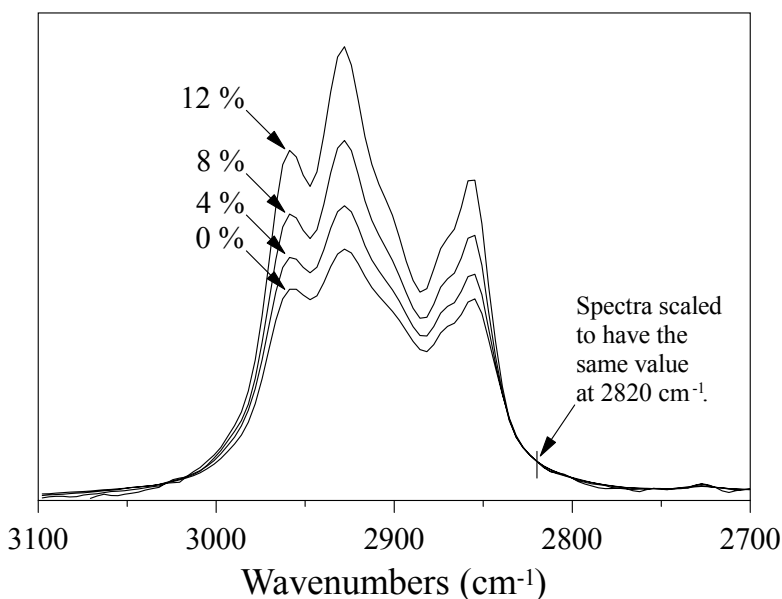


Figure 5. Photoacoustic amplitude spectra of a diesel oil sample containing carbon black loadings from 0 to 12% by weight, which are scaled so that a weak absorption level above that of the carbon black is of equal amplitude for all spectra. All spectra were measured at 2.5 kHz scanning speed. The decreasing spectral saturation with carbon black loading demonstrates conditions in which  $\alpha$  rather than  $L$  defines the sampling depth.

Information provided by PAS magnitude spectra on samples with depth varying composition is complemented by information from the corresponding PAS phase spectra. The phase lag between the infrared excitation and PAS response waveforms is indicative of the depth from which the signal evolves. Consequently, the relative depths from which signals evolve can be determined from the relative phases of their absorbance bands with greater phase lag indicating a greater depth. At lower modulation frequencies, signal-to-noise and background signal problems are less prevalent, and it may be possible to measure phase signals that approach the  $360^\circ$  phase angle limit corresponding to a sampling depth of  $2\pi L$ . In the case of layered samples with strong absorption-band peaks free of spectral overlap from overlayers, it is possible to associate the phase of particular band peaks with either the irradiated face of the sample or the boundaries between layers. The difference in depths,  $\Delta d$ , is related to the difference in phases,  $\Delta\theta_d$ , by equation (11):

$$\Delta d = 2\pi L \Delta\theta_d / 360^\circ \quad (11)$$

as long as the absorption coefficients of the two peaks are similar. Table 2 gives the PAS depth resolution (micrometers per degree) and total PAS sampling depths for different modulation frequencies.

---

Table 2. Angular depth resolution ( $\mu\text{m degree}^{-1}$ ) and maximum sampling depth versus modulation frequency assuming  $D = 10^{-3} \text{cm}^2 \text{s}^{-1}$ .

Modulation frequency, $f(\text{Hz})$	Angular depth resolution $\mu\text{m degree}^{-1}$	Maximum sampling depth $2\pi L(\mu\text{m})$
1	3.1	1120
10	0.98	354
25	0.62	224
50	0.44	159
100	0.31	112
200	0.22	79.2
400	0.16	56.0
1000	0.10	35.4
10000	0.031	11.2

---

Typically, phase spectra are measured with a step-scan FT-IR spectrometer. In phase modulation, the scanning motion of the interferometer is done in a series of steps, rather than smoothly, and an oscillation is added to this stepping motion. The signal produced by this interferometric oscillation is measured at each step. Figure 6 illustrates the vectorial nature of the data. At each step,  $p$ , the oscillation produces a photoacoustic signal of magnitude  $M(p)$  and phase  $\theta(p)$ . The spectrometer measures the in-phase and quadrature components,  $M_0(p)$  and  $M_{90}(p)$ , of this signal, which are the projections of  $M(p)$  onto  $0^\circ$  and  $90^\circ$ :

$$M_0(p) = M(p) \cos(\theta(p)) \quad (12)$$

$$\text{and } M_{90}(p) = M(p) \sin(\theta(p)) \quad (13)$$

The measurements from all of the steps combined make up the in-phase and quadrature interferogram,  $I_0$  and  $I_{90}$ . These then can be separately Fourier transformed to produce the in-phase and quadrature component spectra,  $S_0(\tilde{\nu})$  and  $S_{90}(\tilde{\nu})$ , and the phase-modulation magnitude spectrum,  $S(\tilde{\nu})$  [equation (14)], is then calculated as a power spectrum from these:

$$S(\tilde{\nu}) = (S_0^2(\tilde{\nu}) + S_{90}^2(\tilde{\nu}))^{1/2} \quad (14)$$

The phase spectrum,  $\theta(\tilde{\nu})$ , [i.e., the phase of the photoacoustic signal as a function of wavenumber, equation (15)] can also be calculated from the component spectra:

$$\theta(\tilde{\nu}) = \tan^{-1}\left(\frac{S_{90}(\tilde{\nu})}{S_0(\tilde{\nu})}\right) \quad (15)$$

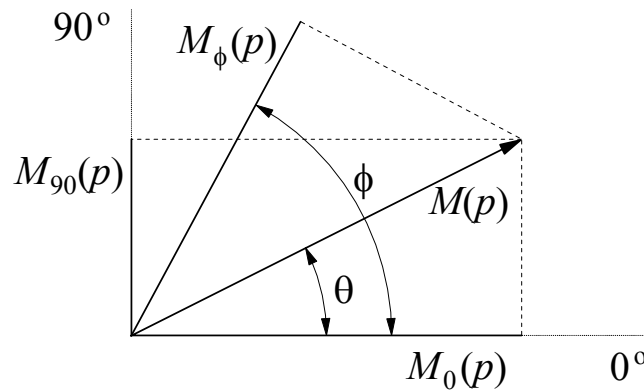


Figure 6. Relationship between a vector magnitude,  $M$ , and phase,  $\theta$ , and its components,  $M_0$  and  $M_{90}$ , as well as its projection  $M_\phi$ , at a phase angle,  $\phi$ . Reproduced from Reference 11.

Often what is required is not the magnitude and phase of the photoacoustic signal, but its projection,  $M_\phi$ , onto a desired angle,  $\phi$ , as illustrated in Figure 6. This is equivalent to measuring the phase-modulation signal with a phase-sensitive detector set to  $\phi$ . This projection can be calculated [equations (16)-(18)] from the in-phase and quadrature measurements:

$$\begin{aligned}
 M_\phi(p) &= M(p) \cos(\phi - \theta(p)) \\
 &= M(p) [\cos(\phi) \cos(\theta(p)) + \sin(\phi) \sin(\theta(p))] \\
 &= M_0(p) \cos \phi + M_{90}(p) \sin \phi
 \end{aligned}
 \tag{16}$$

(17)

(18)

Analogously, the interferogram of the projection onto  $\phi$  is given by equation (19):

$$I_\phi = I_0 \cos \phi + I_{90} \sin \phi \tag{19}$$

$I_\phi$  can then be Fourier transformed to produce the spectrum at angle  $\phi$ , but on some spectrometers this transform will cause artifacts if the Mertz phase correction is used, as is typical. Instead,  $I_\phi$  is Fourier transformed without phase correction so as to produce real and imaginary component spectra,  $S_R(\tilde{\nu}, \phi)$  and  $S_I(\tilde{\nu}, \phi)$ , and the normalized magnitude spectrum at  $\phi$ ,  $S(\tilde{\nu}, \phi)$  [equation (20)], is calculated as a power spectrum from the components:

$$S(\tilde{\nu}, \phi) = (S_R^2(\tilde{\nu}, \phi) + S_I^2(\tilde{\nu}, \phi))^{1/2} / S_B(\tilde{\nu}) \tag{20}$$

where  $S_B(\tilde{\nu})$  is the reference sample spectrum calculated from equation (14).

Thus, once  $I_0$  and  $I_{90}$  are measured in a single FT-IR data acquisition,  $S(\tilde{\nu}, \phi)$  can be calculated at any value of  $\phi$ . It is then possible to calculate three-dimensional plots showing  $S(\tilde{\nu}, \phi)$  as a function of  $\tilde{\nu}$  and  $\phi$ . For layered systems the spectrum of a particular layer is most distinct at a particular value of  $\phi$ . For example, spectra of a 6- $\mu\text{m}$  layer of poly(ethylene terephthalate) (PET), on a polycarbonate substrate are plotted in Figure 7 for the pure components and for the layered sample at phase angles of 75° and 36°. The 75° and 36° spectra can be readily recognized as PET and polycarbonate spectra, respectively.

It is also useful to calculate two-dimensional plots showing how the signal at specific wavenumbers, such as spectral peaks depends on  $\phi$ . These plots have the shape of the absolute value of a sine function, as shown in Figure 8. The phase differences between the plots, 35° in the figure, allow the relative depths of signal evolution to be determined for different bands [using Equation (11)], the ordering of layers to be established, and the grouping together of phase values associated with each layer to be observed.

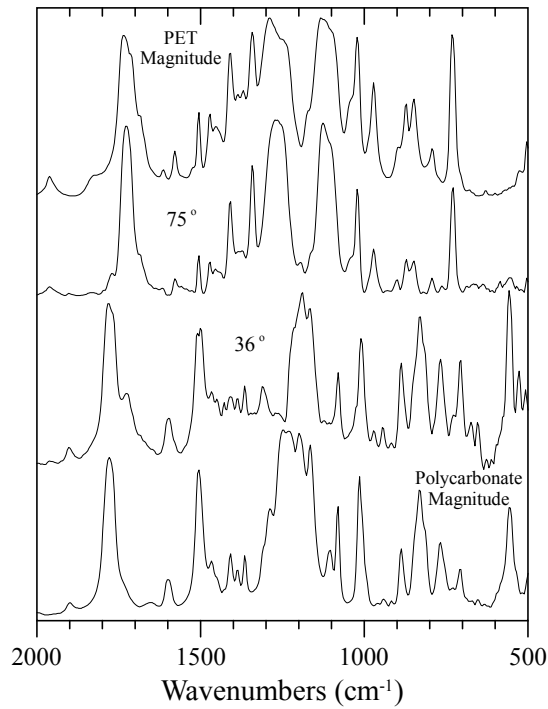


Figure 7. Photoacoustic spectra of a 6- $\mu\text{m}$  layer of PET on a polycarbonate substrate and the pure components. The spectra selected at  $\phi = 36^\circ$  and  $\phi = 75^\circ$  best match the pure spectra of polycarbonate and PET, respectively. The phase values have an arbitrary but common zero.

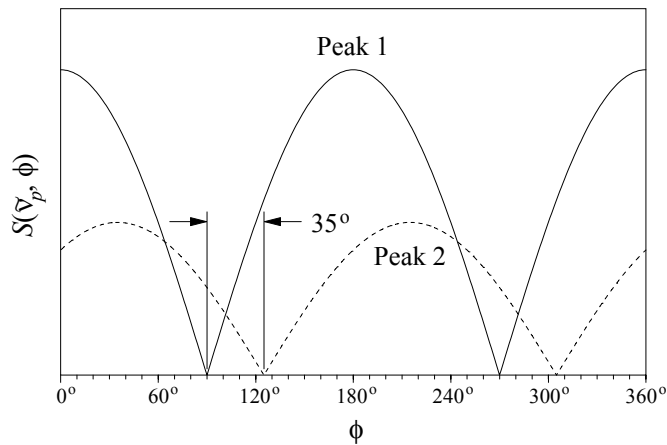


Figure 8. Schematic plot of the PAS amplitude as a function of detection angle for two absorbance band peaks showing a faster evolving signal from nearer the sample surface (Peak 1) and a slower evolving signal from deeper within the sample (Peak 2) with a  $35^\circ$  phase difference between them. The phase scale zero is arbitrary. Note that all of the information is contained in a range of  $180^\circ$ .

The simple signal-generation model for homogeneous samples predicts that the phase lag varies relative to the infrared beam modulation waveform by 90° to 135° as  $\alpha$  goes from very high to very low values.<sup>5</sup> Phases less than 90° are associated with thin layers of lower thermal conductivity on the sample surface or on the sample chamber walls.<sup>12</sup> Phases larger than 135° indicate the presence of an increasing concentration of an absorbing species as a function of depth below the sample surface (gradient) or the presence of layered structures. In the absence of absorption in overlayers, each layer of a layered sample will have a phase ranging over a maximum of 45° that is isolated in phase angle from the other layers, allowing the ordering of layers to be determined.<sup>13</sup> In practice, considerable overlap in spectra from one band to another often exists, but overlayer absorption can be accounted for using a vectorial approach in some instances.<sup>11</sup>

If the phase behavior of samples is to be compared to model predictions, it is necessary to establish the zero phase point that is consistent with the simple signal-generation model because otherwise the FT-IR will assign an arbitrary, but repeatable zero. The zero consistent with the model is determined using a glassy carbon reference sample positioned for the measurement at the same distance below the sample cup rim as the sample being analyzed. The phase of the glassy carbon signal lags the zero point by essentially 90° as discussed in the next section.<sup>6</sup>

It should be noted that the phase spectrum  $\theta(\tilde{\nu})$  given by equation (14) does not track phase angles when they cross quadrant boundaries. In the case of the 0° to 90° quadrant versus the 90° to 180° quadrant, the correct quadrant can be determined by comparing  $S(\tilde{\nu}, 45^\circ)$  and  $S(\tilde{\nu}, 135^\circ)$ . The phase is in the 0° to 90° quadrant and equation (14) pertains if  $S(\tilde{\nu}, 45^\circ) > S(\tilde{\nu}, 135^\circ)$  whereas equation (21)

$$\theta(\tilde{\nu}) = \pi - \tan^{-1}(S_{90}(\tilde{\nu})/S_0(\tilde{\nu})) \quad (21)$$

pertains if  $S(\tilde{\nu}, 45^\circ) < S(\tilde{\nu}, 135^\circ)$ .<sup>11</sup>

A good illustration of the role of sampling depth in PAS is provided by following the PAS phase and magnitude signals versus time as a diffusion front propagates from the rear to front face of a sample.<sup>14</sup> Figures 9 and 10 show the phase and magnitude signals versus time for the strong C-H band at 2920 cm<sup>-1</sup> as a viscous hydrocarbon diffuses through a 254- $\mu\text{m}$  thick porous poly(tetrafluoroethylene) (Teflon<sup>TM</sup>) film. The phase modulation frequencies of the measurements are 25 Hz and 400 Hz resulting in  $L$  ( $2\pi L$ ) values of approximately 36 (226) and 9 (56.5)  $\mu\text{m}$ , respectively, assuming a typical thermal diffusivity value of 10<sup>-3</sup> cm<sup>2</sup>s<sup>-1</sup> for polymers. The phase plot of Figure 9 shows an initial decrease in slope at early times that is likely due to incomplete compensation for a fast phase background signal to be discussed later in this section. Consequently, ignoring the first point in the 25 Hz data and the first 3 points for 400 Hz, results in phase shifts between early in the diffusion and its completion of 330° and 160° for the 25 Hz and 400 Hz data.

Using equation (11), values of 210  $\mu\text{m}$  (5.8L) and 25  $\mu\text{m}$  (2.8L) are calculated for the depths at which the diffusion is first sensed for the 25 Hz and 400 Hz measurements, respectively. The magnitude curves in Figure 10 are not significantly distorted by the



phase background and show clearly that the 25 Hz measurement has greater depth sensitivity as expected than is the case at 400 Hz. Comparison of Figures 9 and 10 show that the phase signal senses the moving diffusion front sooner than the magnitude signal which is commonly the case with detection of subsurface interfaces of both kinetic or static origin.

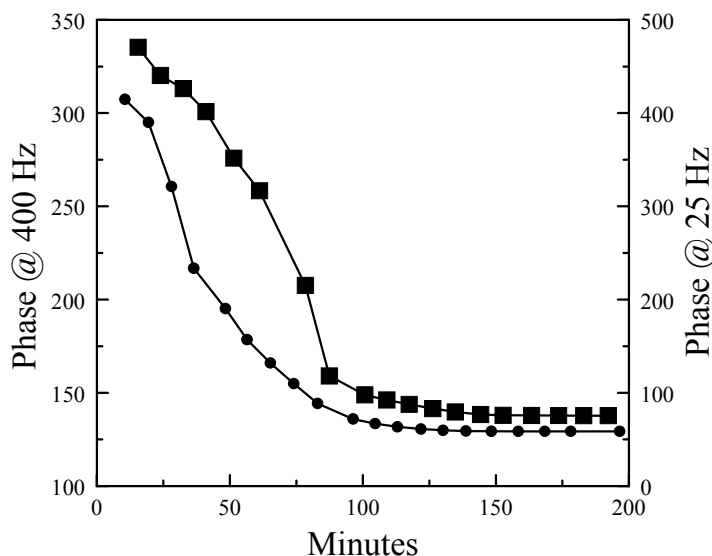


Figure 9. Phase angle of the  $2920\text{ cm}^{-1}$  C-H band of a viscous hydrocarbon versus time during diffusion from the back face to the front face of a  $254\text{-}\mu\text{m}$  thick porous Teflon<sup>TM</sup> membrane measured at 25 Hz (●) and 400 Hz (■) phase-modulation frequencies. The phase scale zero is arbitrary.

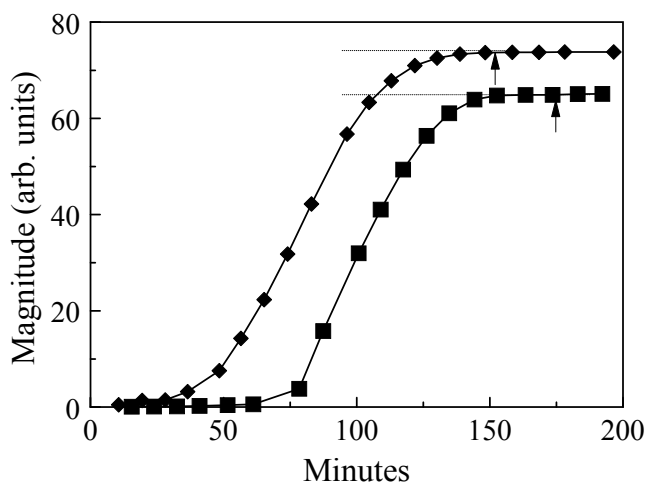


Figure 10. Magnitude of the  $2920\text{ cm}^{-1}$  C-H band of a viscous hydrocarbon versus time during diffusion through a porous Teflon<sup>TM</sup> membrane measured at 25 Hz (◆) and 400 Hz (■) phase-modulation frequencies and plotted on different amplitude scales.

Phase spectra are more susceptible to external interference than magnitude spectra, and this must be kept in mind when interpreting spectra. The total observed photoacoustic signal is the vector sum of all contributions to the signal. This means a small-magnitude interference may have little effect on the magnitude spectrum, yet have a large effect on the phase spectrum if the phase of the signal from the interference differs substantially from the phase of the sample signal. Consider an interference signal that is only one-tenth the size of the signal from the sample, but has a phase that differs by  $90^\circ$  from that of the sample. The interference will change the observed signal magnitude by only 0.5%, but it will shift the observed phase by  $6^\circ$ .

Water vapor and carbon dioxide are the most obvious sources of phase interference. Gas-phase photoacoustic signals are in phase with the light modulation, so they have a phase of  $0^\circ$ , which differs from most condensed-phase-sample signals by at least  $90^\circ$ . There is another interference that is more insidious because it can appear anywhere in a spectrum and its source is far less obvious. This is interference from the small background signal that is virtually always present in FT-IR photoacoustics. Its contribution to the magnitude spectrum is negligible, but its phase differs sufficiently from typical sample phases that it can dominate low-absorption regions of spectra. This background signal comes principally from contamination on the sample and on the sample chamber walls, including adsorbed moisture, the oxides that develop on air-exposed metal surfaces, and generalized contamination. Light absorption by a very thin film of material, especially on a metal surface (or other efficient heat sink), will produce a fast photoacoustic signal whose phase can approach that of the light modulation.<sup>12</sup>

Figure 11 shows both phase and unnormalized-magnitude spectra that demonstrate the effects of interferences. It shows 400 Hz phase-modulation spectra of 2.6-mm-thick polyethylene and poly(methyl methacrylate) (PMMA) disks, which were baked at  $65^\circ\text{C}$  overnight to reduce surface moisture. The photoacoustic detector was purged with helium, and magnesium-perchlorate desiccant was kept in the sample chamber at all times to maintain dryness. The spectra were taken using a Bio-Rad FTS 60A FT-IR spectrometer for which the phase scale is not absolute;  $0^\circ$  is an arbitrary but reproducible point not corresponding to the same phase as the light modulation. On the phase scales in Figure 11, a higher phase corresponds to a later signal. The magnitude and phase spectra were calculated using equations (14) and (21) from the same pair (in-phase and quadrature) of interferograms. The PMMA magnitude spectrum in the bottom panel of the figure (dotted line), shows no interferences larger than the small (about 1 unit tall)  $\text{CO}_2$  doublet at  $2360$  and  $2335\text{ cm}^{-1}$  and no water-vapor structure. Its companion phase spectrum in Figure 11(A), on the other hand, has a prominent (about  $10^\circ$ )  $\text{CO}_2$  doublet and smaller (about  $2^\circ$ ) water-vapor structure between  $1500$  and  $1850\text{ cm}^{-1}$ . The PMMA itself absorbs sufficiently strongly at most mid-infrared wavelengths that the phase effects from the background or surface-film signal are modest. The largest interference from the background signal is the broad,  $9^\circ$ -tall feature between  $3100$  and  $3550\text{ cm}^{-1}$ . This is a common phase-spectrum interference probably caused by water or other hydroxyl species adhering to surfaces. This broad feature demonstrates the apparent phase-band reversal that can result from background-signal interference.

PMMA has a small absorption peak at  $3440\text{ cm}^{-1}$ , which shows up in the phase spectrum as a gap in the interfering hydroxyl feature, so it looks as if the  $3440\text{ cm}^{-1}$  band were pointing toward higher phase instead of lower phase like the other PMMA bands. This is the characteristic appearance of phase interference from the background signal – a broad region of faster than expected phase in which small absorption bands of the sample appear to be partly or fully reversed in direction.

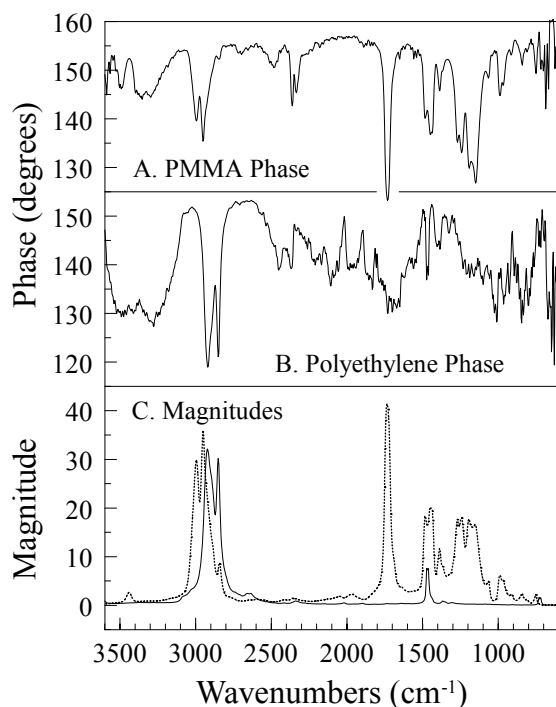


Figure 11. Phase spectra for strongly absorbing PMMA (A) and weakly absorbing polyethylene (B) samples showing the presence of phase background signals as discussed in the text. The phase scale zero is arbitrary. The magnitude spectra are shown for the PMMA (dotted) and polyethylene (solid) samples in C.

Figure 11 also shows a phase spectrum and companion magnitude spectrum (solid line) for polyethylene. Polyethylene has a generally lower absorption away from its main peaks than PMMA does. As a result, its phase spectrum is much more susceptible to background-signal interference. At first glance, the polyethylene phase spectrum appears noisy because there are so many features that apparently have little or no corresponding structure in the magnitude spectrum, but many of the features are real, not random noise. The water interference band between  $3100$  and  $3550\text{ cm}^{-1}$  is again present, and the dip in phase centered at  $1690\text{ cm}^{-1}$  is also probably from superficial water. Many small absorption bands appear reversed in the phase spectrum because of the background interference. The upward-pointing features in the phase spectrum at  $2350$ ,  $2150$ ,  $2020$ ,

1900, 1815, 1360, 1300 and 910  $\text{cm}^{-1}$  all correspond to small absorption peaks in the magnitude spectrum. Phase spectra contain much useful information complementary to magnitude spectra, but the background interferences can make phase spectra more difficult to interpret in weakly absorbing spectral regions, especially at high modulation frequencies.

## Instrumentation

The utility of FT-IR PAS depends significantly on the performance of both the photoacoustic detector and the FT-IR spectrometer. Optimization of both can be critical in demanding applications because of the thermal-wave reflection problem mentioned in the previous section, which leads to low acoustic signal levels and vulnerability to noise interference. Optimization is especially necessary when shallow sampling depths are required. In this case, the amount of detected energy is low because of the thinness of the layer being probed, and this leads to very low signals.

The two major noise sources in FT-IR PAS measurements are structure-borne vibration, which couples to the microphone, and electronic noise. These can be controlled by design considerations and careful choice of the microphone and preamplifier components, but there are practical limitations. Consequently, in terms of the FT-IR spectrometer, a high intensity infrared source, low  $f$ -number optics, a stable mirror velocity to reduce interferometer-induced noise in the IR beam modulation, and control of mechanical vibrational resonances associated with the optical bench are all very important.

The main PAS detector design considerations can be divided into two categories: signal enhancement and noise suppression. The former includes an optical design to focus all of the available IR energy onto the sample, restricting the gas volume to just suffice for signal generation with minimal excess, provision for helium gas purging of the sample chamber to enhance the transfer of heat to the gas and boost the signal generation efficiency by approximately a factor of 3 over signal generation in air, and use of a high sensitivity microphone with a typical value of 50 mV/Pa.

The noise suppression factors include both avoiding and damping mechanical resonances in the detector housing and support structure as much as possible, supporting the detector housing on vibration isolators, using limp cables and purge tubing to reduce propagation of vibration along these paths to the detector, employing seals and a window design that make the detector as immune as possible to air-borne noise, and use of a low noise preamplifier.

Most commercial FT-IR PA detectors currently in use are products of MTEC Photoacoustics, Inc.,<sup>15</sup> manufacturer of the Model 100, 200, and currently the Model 300 instruments. The newest MTEC Model 300 units reflect the present trend in FT-IR accessories by mounting on a pre-aligned FT-IR-specific baseplate, as shown in Figure 12, and having, in the case of the system shown, a computerized FT-IR PAS tutorial to instruct the user. The detector has an optical path leading to the detector that is sealed

from the room atmosphere on purged FT-IR systems. The spectral range of a PAS system is defined by the transmission range of the detector's sample-chamber window and by the spectral range of the FT-IR instrument. Most FT-IR PAS measurements are made in the mid- and near-infrared spectral regions.

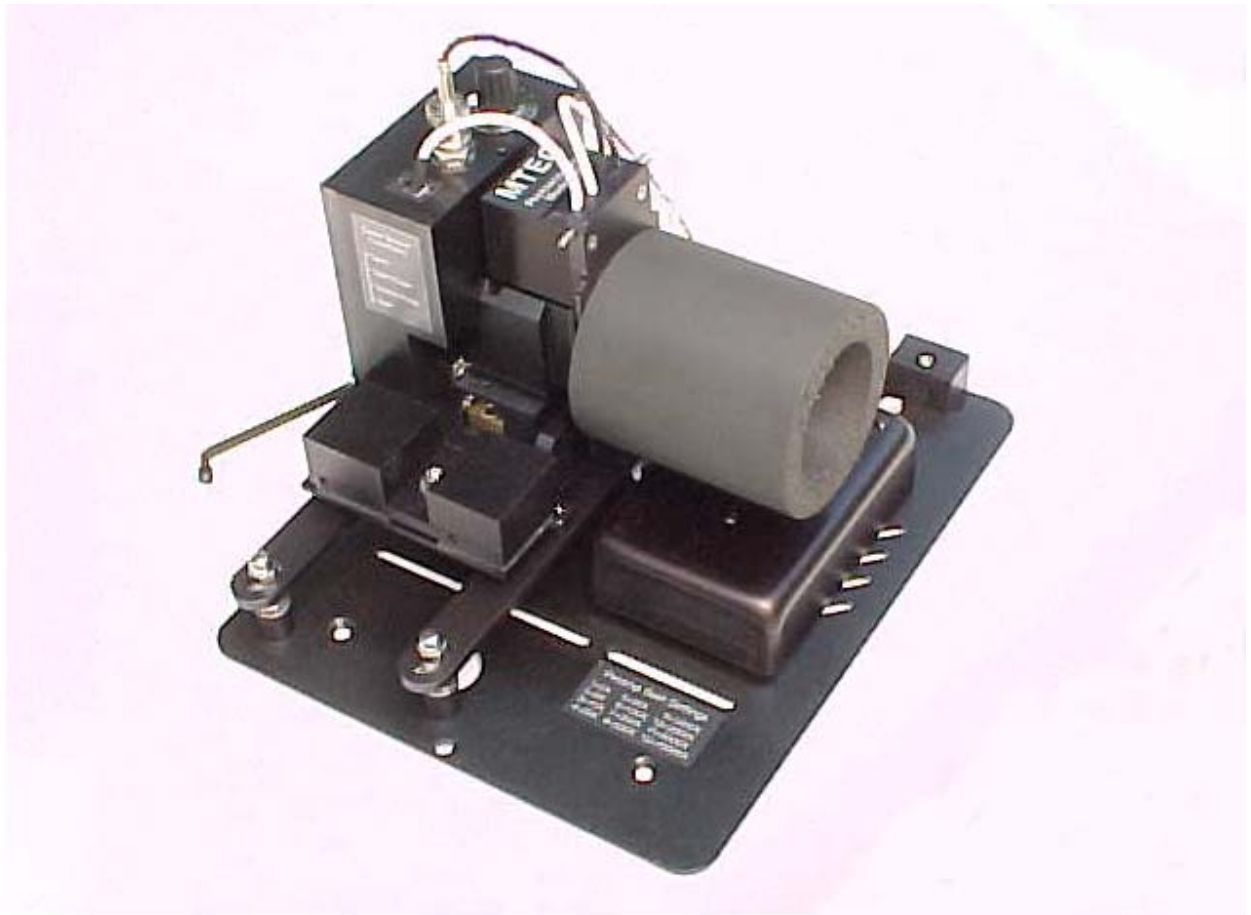


Figure 12. Photograph of an MTEC Photoacoustics Model PAC300 Nicolet ESP photoacoustic detector, which incorporates automatic accessory recognition and set-up.

MTEC sample holder cups accept samples as large as 10 mm in diameter by 6 mm thick. The IR beam is focused into a 5-mm-diameter area in the center of the cup in MTEC detectors. This consideration, combined with the fact that the signal evolves from a sample depth of well under a millimeter, indicates that much smaller samples than the holder cup size are adequate to produce the maximum signal level possible for a particular material. If suitably sized specimens are not available, they are typically produced using a punch, razor blade, scissors, file, abrasive or other means of size reduction. MTEC detectors have stainless steel sample cups that insert into the holder cup for holding such samples and spacers to displace extra gas volume that would otherwise reduce the signal magnitude.

The use of helium gas (zero grade or better) and of desiccant to reduce water vapor and CO<sub>2</sub> in the sample chamber are desirable to ensure reproducibility, to optimize signal-to-noise, and to avoid spectral interferences. PAS detectors have provision for purging to establish a helium atmosphere in the sample chamber. Water vapor and CO<sub>2</sub> that evolve from some samples during measurements are best controlled with magnesium perchlorate for water vapor and molecular sieve spheres for CO<sub>2</sub>. Using small amounts of sample also helps to reduce the load on the desiccant, which is placed in a cup underneath the sample cup of the sample holder.

FT-IR PAS magnitude spectra must be normalized to remove spectral features due to the IR source, optics, and PAS detector response by dividing the sample spectrum by the spectrum of a sample that ideally would be 100% absorbing over the entire spectral range. MTEC provides a carbon-black-coated-reference sample<sup>15</sup> for this purpose. It is designed to have a very low thermal mass and generate a much stronger signal than the typical sample. Consequently, a relatively small number of co-added scans of the FT-IR produce a reference spectrum with a high signal-to-noise ratio so that the final signal-to-noise ratio of a normalized spectrum is typically dominated by the sample spectrum's quality.

In special situations, the carbon-black-coated-film, however, is not the preferred reference and either self-referencing or a glassy-carbon disk<sup>15</sup> reference is more suitable. Self-referencing is desirable for samples that are themselves very strongly absorbing. For instance, the spectra of adsorbates on carbon black can best be referenced by strongly smoothing a copy of the sample spectrum to wash out adsorbate band features and then dividing the sample spectrum by its smoothed counterpart. An additional spectral subtraction step follows to complete the normalization in which the normalized spectrum of the carbon black before treatment with an adsorbate is subtracted from the normalized spectra of treated samples to remove any sharp instrumental spectral features appearing in the sample spectrum not associated with the adsorbate. This approach allows different sample treatment processes to be studied using one-for-one spectral subtractions in spite of sample thermal response variations that may be caused by differences in processing of the sample. The absorbance bands of spectra obtained by this method have a somewhat derivative character but still have better possibilities for analysis purposes than other data treatment approaches for this difficult to characterize class of samples.

The other special referencing situations require the use of a glassy carbon disk in order either to avoid low frequency response problems with the carbon-black-coated-film

below a modulation frequency of approximately 5 Hz or to provide a phase reference to account for instrumental phase changes when both phase and magnitude data are being utilized. As discussed earlier, the phase angle of the PAS signal corresponds to the angular shift between the IR beam excitation waveform and the photoacoustic signal response waveform, which is delayed in time due to the finite thermal-wave propagation time during signal generation. According to theory for homogeneous samples, the PAS signal phase equals  $90^\circ$  when the product  $\alpha L$  is very large ( $\geq 1000$ ), as with very strongly absorbing samples, and approaches  $135^\circ$  when  $\alpha L$  is very small. The ideal phase reference should have a very high  $\alpha$  across the complete spectral region of interest so that the  $\alpha L$  product will be very large for all  $L$  values of interest and the photoacoustic phase of the reference will be a constant  $90^\circ$ . The phase spectra of some candidate materials as well as a homogeneous polyethylene terephthalate (PET) sample are shown in Figure 13 on a phase scale axis with the same but arbitrary zero for each spectrum. The data shown supports the use of glassy carbon as a phase reference because the PET phase spectrum is always within  $45^\circ$  ( $135^\circ$ - $90^\circ$ ) of the glassy carbon spectrum and the PET phase never leads the glassy-carbon phase. The glassy-carbon spectrum also maintains a constant phase versus wavenumber consistent with theory.

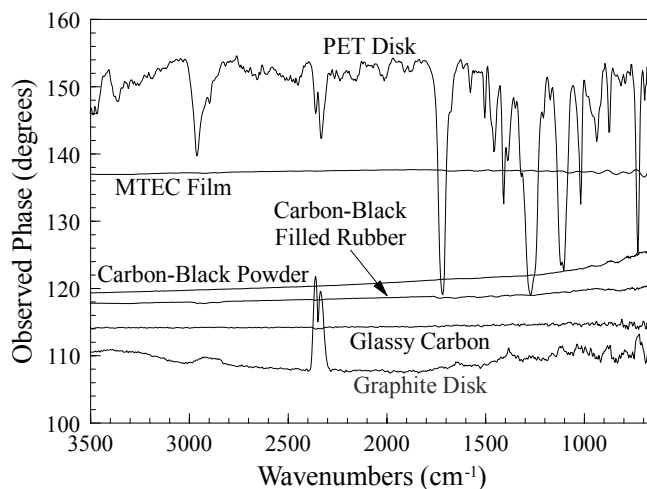


Figure 13. Phase spectra for five candidate phase reference materials and PET. The phase scale zero is arbitrary.

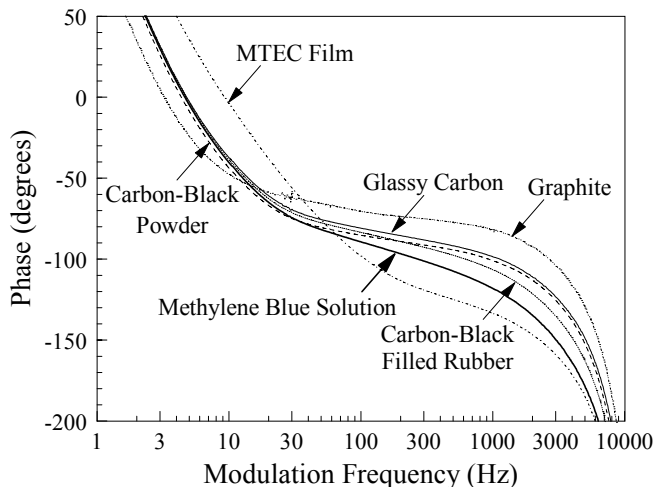


Figure 14. Phase versus modulation frequency for five candidate phase reference materials and a methylene-blue solution sample. The phase scale zero is coincident with that of the excitation waveform.

Figure 14 shows the phase response on an absolute scale of the candidate reference materials as a function of frequency. These data were measured using a sinusoidally modulated red light emitting diode (LED) light source and include data on a methylene blue solution ( $\alpha \cong 2000 \text{ cm}^{-1}$ ). The reference materials, according to theory, cannot have phases that lead the solution sample by more than  $45^\circ$  and should have a phase of  $90^\circ$  independent of frequency, if the frequency response of the detector were not present. The curves in Figure 14 diverge from theory toward faster phase angle at low frequency because the microphone loses sensitivity and because the thermal wave propagating in the helium atmosphere “shorts out” at the detector window and walls with a gas layer thickness, in this case, of approximately 6 mm. At the high frequency end the signal response diverges toward slower phase angle because the detector has a resonance just below 10 kHz. The curves for carbon black, graphite and the MTEC film do not conform to theory because they have a slower phase in certain frequency regions than the methylene blue solution.

The final data supporting the choice of glassy carbon as a phase reference over carbon-filled rubber is shown in Figure 15. The theoretical curve was calculated for the methylene blue solution and experimental curves were calculated from the data in Figure 14 to test how well the glassy carbon and carbon-filled rubber references remove frequency dependence not related to the sample from the data. Neither of the materials behaves exactly as the ideal  $90^\circ$  phase reference but the glassy carbon is within  $5^\circ$  of the ideal over the range from 1 Hz to 10 kHz, whereas the rubber diverges by as much as  $20^\circ$ .



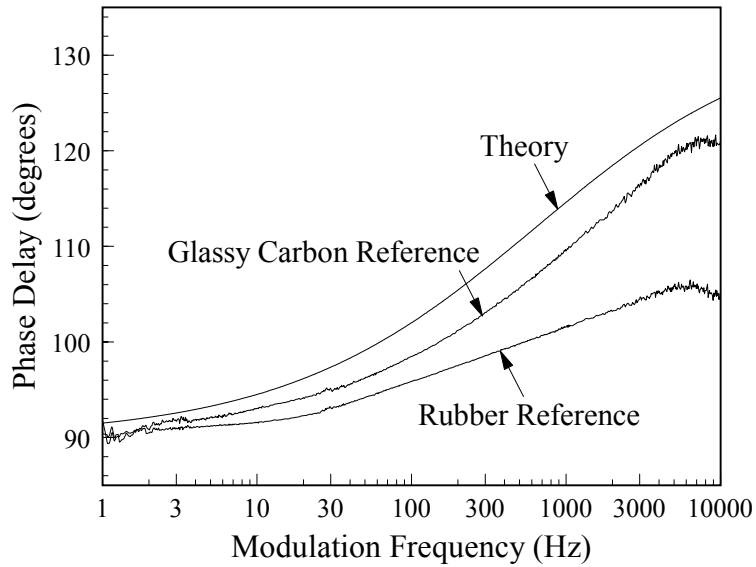


Figure 15. Phase versus modulation frequency for a theoretically calculated curve for methylene blue and for experimental phase data on methylene blue plotted using the glassy carbon and carbon-black filled rubber as phase references. The phase scale zero is coincident with that of the excitation waveform.

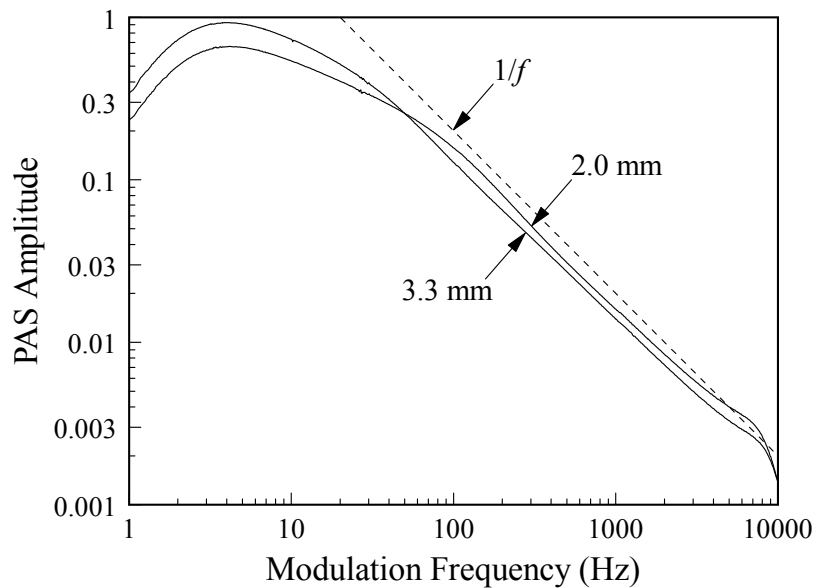


Figure 16. Plot of the photoacoustic signal magnitude versus frequency measured with a Model PAC300 MTEC photoacoustic detector and glassy carbon reference.

The frequency range of PAS measurements is limited by the frequency response of the detector. The frequency response of the PAS magnitude signal for the MTEC Model 300 detector is shown in Figure 16 with a glassy carbon sample and with gas layer thicknesses of 2 and 3.3 mm between the sample and window. Theoretically, the slope of the plot should be  $-1$  but low and high frequency roll-offs are seen for the same reasons described in the frequency plots for the phase signal. The glassy carbon signal shows a slope of  $-0.95$  over its linear range for both sample positions in close agreement with theory. The plot indicates that measurements can be made over the frequency range from less than 1 Hz to nearly 10 kHz, which correspond to FT-IR mirror velocities of about 0.0016 cm/s (25 Hz on the HeNe laser fringe) to 2.5 cm/s (40 kHz) in the spectral range of  $400\text{ cm}^{-1}$  to  $4000\text{ cm}^{-1}$ . The fingerprint region below  $2000\text{ cm}^{-1}$  can also be accessed at 5 cm/s (80 kHz).

After the FT-IR velocity has been chosen to provide the desired sampling depth, the PAS detector gain should be set to provide a signal level that produces a centerburst amplitude that does not exceed the range suitable for the FT-IR's analog to digital converter. Usually, a peak-to-peak amplitude well below 10 V is desirable. The signal level produced may be considerably less even at the highest setting for high modulation frequencies and/or for weak signal generating samples such as polyethylene. In many instances, it is possible to use the same gain setting at a given mirror velocity for both the sample and reference spectra in spite of the considerably higher signal of the latter. A custom of using a common gain setting whenever possible makes it easier to compare spectra without having to account for gain setting differences in normalized spectra.

The spectrometer is the other important component in photoacoustic instrumentation. A multiplexed spectrometer, such as a commercial FT-IR instrument, is highly desirable because of its signal-to-noise ratio advantage, which is also enhanced by the absence of throughput-reducing slits common to dispersive spectrometers. FT-IR spectrometers provide a wide range of modulation frequencies controlled by the interferometer without the acoustic noise of most optical choppers. Continuous scan FT-IR spectrometers can produce modulation frequencies of practical use from less than 1 Hz to 10 kHz in the mid-IR. In the continuous-scan mode of FT-IR operation, the frequency increases with wavenumber by a factor of ten going from  $400\text{ cm}^{-1}$  to  $4000\text{ cm}^{-1}$ , resulting in approximately a factor of three reduction in  $L$ . Step-scan FT-IR spectrometers have the advantage of phase modulation, which results in a constant modulation frequency across the spectrum and easier access to the phase of the PAS signal. The modulation frequency range of step-scan instruments is nearly as wide as continuous-scan FT-IR spectrometers, if the higher harmonics of the phase modulation can be accessed, although there is some compromise of signal-to-noise ratio with a step-scan versus continuous-scan FT-IR measurement.

A number of specific FT-IR operating parameter settings are important in optimizing FT-IR PAS measurements. Spectral resolution should be set as low as is practical because when resolution is reduced by a certain factor the signal-to-noise ratio improves linearly by that factor for a given measurement time. Thus, changing from  $4\text{ cm}^{-1}$  to  $8\text{ cm}^{-1}$  resolution reduces the measurement time by a factor of four. Many

analyses on solids and liquids can be readily done at 8 cm<sup>-1</sup>, 16 cm<sup>-1</sup>, or 32 cm<sup>-1</sup> resolution, although it has often been the custom to work at 4 cm<sup>-1</sup>. In PAS measurements, 4 cm<sup>-1</sup> resolution can rarely be justified, especially since it may require reduction of the source aperture. An open aperture is always preferable in PAS measurements.

The range of modulation frequencies used in PAS measurements is of particular importance when depth-specific chemical information is required and when the sample is weakly absorbing, as in the near-IR, in which case mirror velocities of 0.006 cm/s (100 Hz for the He-Ne laser line) or lower are best suited. Three possibilities exist for generating a range of modulation frequencies with an interferometer. The most common is continuous-scan modulation, where the optical path difference (OPD) velocity,  $V$ , is constant, and the modulation frequency,  $f$ , at a particular wavenumber,  $\tilde{\nu}$ , is given by  $f = V\tilde{\nu}$ . Table 3 summarizes the modulation frequencies that can be obtained in the near-, mid-, and far-IR spectral regions. The table lists the scanning speed velocities to be selected as an FT-IR parameter in terms of the two units commonly used. They are the OPD velocity (in cm/s) or the He-Ne laser modulation frequency  $f_l$  (in Hz), which is related to  $f$  by  $f = \tilde{\nu}f_l/15803$  cm<sup>-1</sup>.

Table 3. FT-IR modulation frequencies generated by different OPD velocities (Hz).

OPD Velocity		far IR	mid IR	near IR	visible-UV	
cm/s	Hz	50 cm <sup>-1</sup>	400 cm <sup>-1</sup>	4000 cm <sup>-1</sup>	10000 cm <sup>-1</sup>	50000 cm <sup>-1</sup>
0.00316	5			1.27	3.16	15.8
0.00633	10			2.53	6.33	31.6
0.0158	25			6.33	15.8	79.1
0.0633	100		2.53	25.3	63.3	316
0.0253	400	1.27	10.1	101	253	1270
0.0506	800	2.53	20.2	202	506	2530
0.158	2.5k	7.91	63.3	633	1580	7910
0.316	5k	15.8	127	1270	3160	15800
0.633	10k	31.6	253	2530	6330	
1.27	20k	63.2	506	5060	12700	
2.53	40k	127	1010	10100		
5.06	80k	253	2020			
7.59	120k	380	3040			

The second method of IR beam modulation, called phase modulation,<sup>16,17</sup> is done in the step-scan mode of FT-IR operation where the OPD is scanned in a series of incremental steps. Phase modulation of the infrared beam intensity occurs when the position of one of the interferometer mirrors is oscillated about the step locations with an amplitude that is measured in terms of the wavelength of the instrument's helium-neon laser. The mirror oscillation produces a modulation of the IR beam intensity at a constant frequency for all wavenumbers in contrast to continuous-scan modulation. Hence, the sampling depth defined by thermal-wave decay is constant across the spectrum. The PAS signal produced by phase modulation is converted typically by the digital signal processing (DSP) electronics of the FT-IR spectrometer into in-phase and quadrature interferograms that can be processed to obtain magnitude and phase spectra. If the mirror oscillation has a square waveform, the IR beam is modulated at the fundamental frequency and at higher frequency odd harmonics of the fundamental. This allows spectra measured at several sampling depths to be obtained in a single acquisition.

The use of phase modulation results in the presence of minima and maxima structure in the modulated IR beam intensity as a function of wavenumber. The presence of a minimum at a particular wavenumber prevents the measurement of PAS spectra due to the low modulation efficiency at and near the minimum wavenumber location. The wavenumber locations of the maxima,  $\tilde{\nu}_p^{max}$ , and minima,  $\tilde{\nu}_p^{min}$ , are given by equations (22) and (23):

$$\tilde{\nu}_p^{max} = 15,803 (p-1/2)/n \quad (22)$$

and 
$$\tilde{\nu}_p^{min} = 15,803 p/n \quad (23)$$

where  $p$  is the number of the maxima or minima and  $n$  is the number of helium-neon laser wavelengths corresponding to the mirror oscillation amplitude. In most instances,  $\tilde{\nu}_p^{min}$  is chosen to be somewhat above the high wavenumber limit of the spectral range of interest. Since equations (22) and (23) do not account for the possibility of shifts in the minima and maxima due to certain optical and electronic characteristics unique to a particular FT-IR instrument, it is advisable to experimentally verify the suitability of the  $n$  value selected with these formulas using a carbon black film or other reference sample.

The third method of IR beam modulation exploits the impulse modulation that can be generated as the mirror position is incremented to generate the retardation change in the step-scan mode of operating an FT-IR spectrometer.<sup>18,19</sup> This step impulse produces an IR beam modulation containing a wide range of Fourier frequencies. The photoacoustic response to the impulse can be processed to produce time-resolved spectra. Due to the finite propagation time of thermal waves, the spectra observed represent deeper layers of the sample as the time interval after excitation increases.

The PAS signal generated by the impulse is a convolution of spectral and frequency components due to the sample, as well as to the source, interferometer, detector, microphone, and electronics. Normalization for the convolution of these latter signal components is necessary in order to obtain information on the sample alone. The total convoluted signal,  $S(t)$ , including the sample and other components can be expressed

as a convolution function,  $S(t) = s(t) * B(t)$ , where  $s(t)$  is the sample component,  $B(t)$  is the signal measured with a black reference sample such as glassy carbon, and the  $*$  symbol denotes a convolution rather than a multiplication. A Fourier transform of the time domain function produces a spectrum of the signal in the frequency domain,  $S(\omega) = s(\omega)B(\omega)$ . Solving for  $s(\omega) = B(\omega)/S(\omega)$  and taking the inverse Fourier transform yields the actual time response of the sample alone [equation (24)]:

$$s(t) = F^{-1}[S(\omega)/B(\omega)]. \quad (24)$$

This process is repeated at each retardation step resulting in an array of sample time decay signals as a function of retardation, similar to the process common in other time-resolved spectroscopy (TRS) measurements. A TRS shuffle of the data reorganizes the array into a series of interferograms, which are converted into time-resolved spectra.

The last FT-IR consideration specific to PAS relates to the time required to acquire a spectrum with the desired signal-to-noise ratio. Spectra can be acquired with a minimum number of scans by running at the lowest mirror velocity and resolution appropriate for the analysis and by using an open aperture and helium purge. For example, qualitative identification of polymers can be done with a single scan at 0.1 cm/s mirror velocity and 16  $\text{cm}^{-1}$  resolution. On the other hand, observation of organics adsorbed on carbon black powder may require tens of thousands of scans or more in order to observe very small features superimposed on a very strong background signal.

Several items of instrumentation, in addition to the PAS detector and spectrometer, can be employed to advantage in special circumstances. If diffuse reflectance and transmission spectra are needed to complement PAS measurements, MTEC supplies interchangeable sampling heads for PAS detectors that allow these spectra to be measured.<sup>2,15</sup> Such measurements are often useful to provide greater bulk sensitivity. Sampling heads are also available from MTEC to mount single particles on tungsten needle supports or single fibers on support rings.<sup>2,15</sup>

Samples with compositional gradients or layered structure can be studied by varying the sampling depth but the spectra obtained cannot currently be converted into compositional profiles without additional information. A microlapping method can be employed to produce profiles when such information is not available or when the depth of interest exceeds the decay distances of the beam and/or thermal waves. In these cases the microlapping device<sup>15</sup>, shown in Figure 17, allows planar samples to be analyzed with a spatial resolution of several micrometers. Compositional profiles are measured by initially measuring the spectrum at a shallow sampling depth and then removing a few micrometers using the microlapping device. This sequence is repeated until the sample's composition versus depth has been determined to the desired depth.



Figure 17. MTEC MicroLap equipment for removal of several micrometer increments of material from layered or gradient materials allowing chemical species profiles to be determined to arbitrary depths.

## Sample Considerations

PAS sampling is often used without a second thought because it is simple to quickly obtain a spectrum of nearly any type of sample. For many qualitative analyses of homogeneous samples this is appropriate, but for more complicated samples, there are a number of considerations that are important to be aware of.

Samples that are inhomogeneous should always be evaluated to define a suitable protocol, which assures that the data is representative of the whole sample or of the region of interest. For whole sample analysis, a fine or coarse powdering of the sample may be necessary followed by splitting out and analyzing triplicate samples to check reproducibility. In other cases, it may be necessary to average the spectra of a number of randomly selected samples three times and then check for repeatability until the number of samples is large enough so that their averaged spectra produces a repeatable result within the limits required.

When a small region of the sample is to be analyzed, aluminum foil can be used to mask the area of the sample that is not to be analyzed, or the region of interest can be excised for analysis using a scalpel or diamond file. Extraction is also a useful approach with PAS analysis if soluble components need to be separated from carbon black, which is useful in tire analyses. The solvent containing the dissolved sample can be decanted off after the carbon black settles out. The decanted solution is then placed in a disposable thermal analysis cup and the solvent is evaporated off leaving a residue of the components of interest for analysis without the carbon-black background.

PAS analysis of liquid samples primarily involves situations where the sample is unsuitable for transmission measurements due to high opacity, high viscosity, suspended components, risk of cross contamination, and/or the desire to avoid the clean-up requirements of sample cells. PAS sampling of liquids usually uses disposable cups, which eliminates cross contamination and clean-up problems. Special care is needed with PAS analysis of liquids if the liquid has suspended components or is volatile. Suspended components often settle with time as, for example, in the case of soot in diesel oil. Consequently, if these components are being analyzed, it is important to be sure that they are homogeneously distributed when the sample is placed in the cup and that they remain so during the analysis. FT-IR PAS spectra of liquids should be checked for a vapor phase component by putting a metal disk over the sample. This prevents the IR beam from reaching the sample but allows the vapor above the sample to absorb the beam and produce a vapor spectrum. This vapor spectrum can be subtracted from the spectrum measured with the disk removed to produce a spectrum purely of the liquid.

The use of a disk over the sample is also useful with solids if the analysis of evolved vapors is required. In this case, higher sensitivity will be realized with a larger amount of sample and a longer waiting time for the vapor concentration to increase. In other instances, it is of interest to prevent the evolution of vapor from the sample while measuring the spectrum, such as with hydrated tissue specimens. In this case, it is possible to seal the sample in a vapor-tight cup with a 10- $\mu\text{m}$ -thick polyethylene membrane window in contact with the sample. The thin window allows the thermal

wave generated in the sample to be transmitted to the gas where the PAS signal is generated.

Samples with very low absorption or with very high absorption require special considerations. Low-absorption conditions are common in near-IR analyses and in low-concentration measurements. In both cases, it is necessary to use low mirror velocities to increase the sampling depth and the fraction of the IR beam energy that excites the PAS signal. In the case of very highly absorbing sample conditions, such as analysis of adsorbates on carbon black, very high signal-to-noise ratio spectra are required, which are then normalized using the method of self-referencing described in the discussion on normalization of spectra. If the signal-to-noise ratio is not sufficient, the bands of interest will be dominated by noise when the spectrum is expanded on the ordinate axis to observe these weak features. In some instances, absorbance bands of adsorbates on very strongly absorbing materials appear reversed in spectra as negative-pointing bands. The mechanism for this has not been fully explored, but it appears that a PAS signal from the black substrate, which produces a transmission spectrum after the IR beam passes through the adsorbate, is larger than the PAS signal from the adsorbate itself.

Microsamples, such as films that are thinner than  $2\pi L$  and free-standing (gas on both sides), display magnitude and phase responses that are very different from thick samples. Figure 18 shows the calculated magnitude and phase signals as a function of modulation frequency for a range of film thicknesses with an absorption coefficient of  $10^4 \text{cm}^{-1}$ , a typical value for a strong absorbance peak. The magnitude signals are plotted as a ratio relative to the signal of a 2-mm-thick sample to best illustrate the signal enhancement effect common to thin samples. The enhancement is due to the multiple passes that the thermal waves make within the sample as a result of the very high reflectivity of solid-to-gas interfaces. The multiple passes lead to multiple thermal transfers into the gas and a larger signal. This enhancement effect is what makes microsample analyses possible in PAS in spite of the very small area that single fiber and single particle samples present to the IR beam. Single fibers, 10  $\mu\text{m}$  in diameter and less, are practical for analysis as well as single particles of 50  $\mu\text{m}$  and larger sizes.

The phase signals shown in Figure 18 also show the effect of multiple thermal-wave reflection within thin samples. In the case of phase, the signal is delayed in its evolution at lower frequencies because  $2\pi L$  increases as the frequency decreases. This results in many passes of the thermal waves back and forth within the sample at low frequencies before decaying away and a corresponding delay in the signal evolution. The phase signal is seen to vary between  $90^\circ$  and  $135^\circ$  as expected for a single homogeneous layer.

A final comment on thin film samples is that PAS spectra of these materials are free of the optical interference fringes, which are observed in transmission and reflection spectra. The absence of fringes in PAS spectra makes it much easier to observe weak features due to additives in polymer film spectra.

Gradient and layered samples are discussed in detail in the second section and, in the case of layers, in the next section, and are, therefore, not covered here.



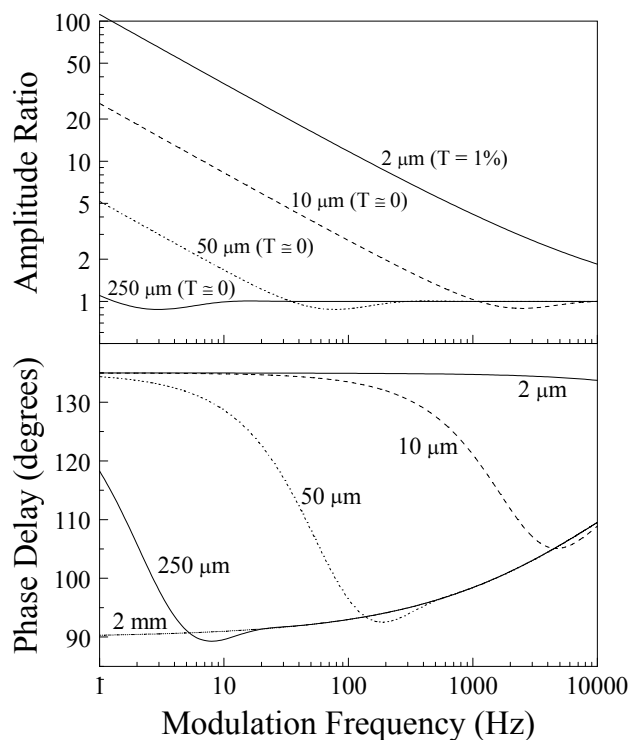


Figure 18. Magnitude and phase signals versus frequency calculated for thin free-standing films of different thicknesses. The magnitude ratio is relative to the signal of a 2-mm-thick sample. The phase scale zero is coincident with the excitation waveform zero.

## Applications

The FT-IR PAS technique is used extensively in industrial and other laboratories on a wide range of applications. Its main value for the majority of users is the ease by which FT-IR spectra can be measured on nearly any sample without sample preparation. The second important value to the user is the ability of FT-IR PAS to provide a better understanding of materials with depth varying compositions.

Six applications will be presented, with each one typical of a particular area of application or of an important consideration in FT-IR PAS measurements. The applications include:

1. Process characterization. In this case following paint cure as a function of baking temperature.
2. Qualitative and quantitative analysis of woods of various tree species.
3. Increasing surface specificity by linearizing the FT-IR PAS signal to observe a surface treatment on fibers.

4. Analysis of the 6-  $\mu\text{m}$  PET layer on polycarbonate sample discussed earlier (see Figure 7) to further illustrate the use of magnitude and phase information on a layered sample.
5. Analysis of a microsample consisting of a single fiber with a polymer coating.
6. Analysis of a three-component sample with layer thicknesses too thin for cross-sectional analysis by FT-IR microscopy.

#### Application 1.

Automobile paint finishes are processed in a baking oven that causes the cure chemistry to progress to the desired point. The spectra in Figure 19 show how the cure varies for different oven temperatures and how paint samples can be tested to verify that the correct cure level is reached. The spectra were measured by continuous-scan FT-IR spectroscopy at 2.5 kHz and  $8\text{ cm}^{-1}$  resolution.

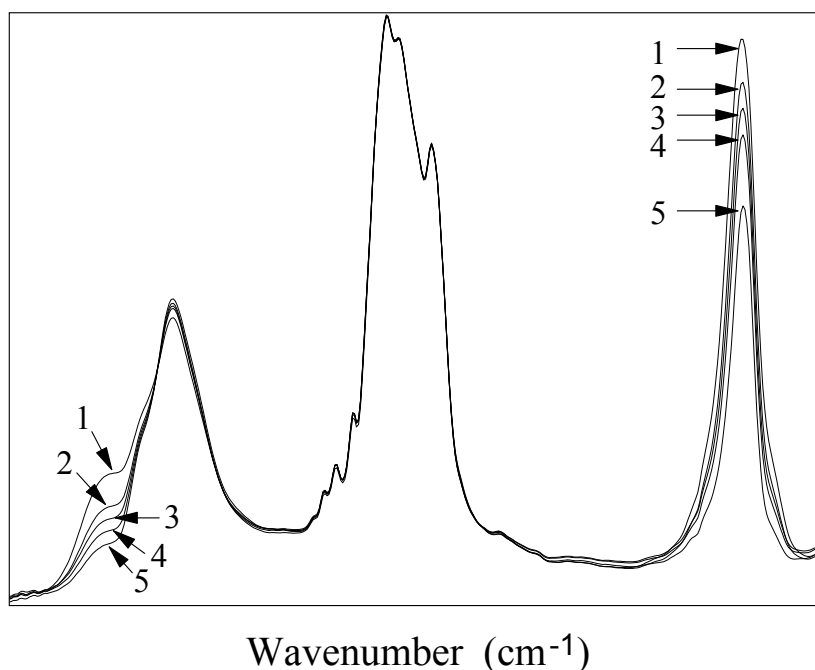


Figure 19. Photoacoustic spectra of a paint processed at five cure oven temperatures, (1) under bake,  $220^{\circ}\text{C}$ , (2)  $250^{\circ}\text{C}$ , (3)  $265^{\circ}\text{C}$ , (4)  $285^{\circ}\text{C}$ , and (5) over bake,  $325^{\circ}\text{C}$ . The wavenumber scale is not enumerated due to proprietary concerns.

## Application 2.

In this study, wood from seven species of trees were analyzed to distinguish between hardwoods and softwoods, and between different species. Determinations were also made of hemicellulose, lignin, glucan, and extractives in the woods. FT-IR PAS can easily measure spectra of single slab specimens, but in order to get the necessary sampling statistics, the wood samples were ground into fine powders and split into sub-samples for analysis. Spectra were measured in the mid-IR at 2.5 kHz and  $8\text{ cm}^{-1}$  resolution. Partial least squares (PLS) analysis was used to analyze the FT-IR PAS spectra for both qualitative and quantitative purposes. In the case of qualitative analysis, samples can be differentiated by tree species based on their PLS principal component scores. Figure 20 plots the scores for the second and third principal components, which separates hardwoods from softwoods. Plotting the first and fifth components (not shown) splits the softwoods into two groups, one of which contains Douglas Fir, Ponderosa Pine, and White Fir. Figure 21 shows how the fourth and fifth components allow this group to be differentiated at the species level. Figures 22 and 23 show the quantitative results for hemicellulose and lignin, respectively.

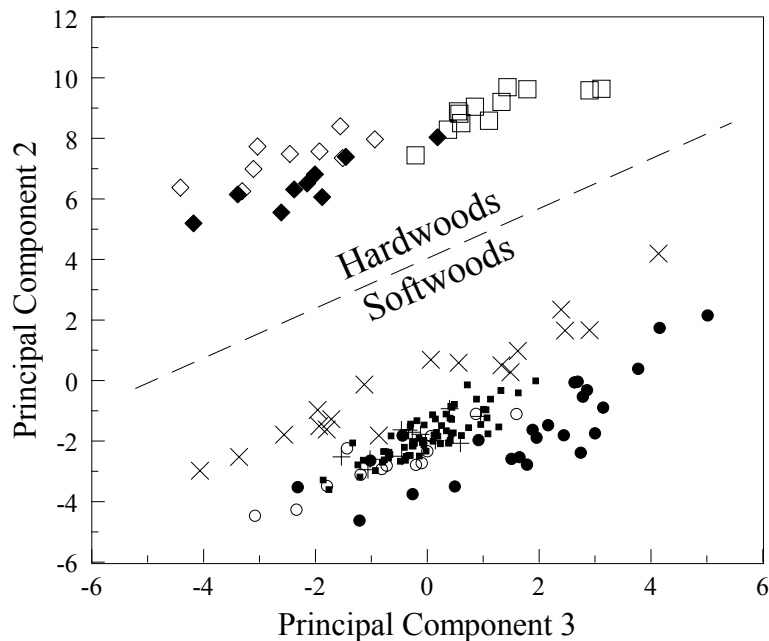


Figure 20. Plot of PLS principal components 2 versus 3, showing the differentiation between hardwoods and softwoods based on their FT-IR PAS spectra. The tree species (symbol) are: Acacia ( $\times$ ), Douglas Fir ( $\square$ ), Eucalyptus ( $\odot$ ), Loblolly Pine ( $\square$ ), Ponderosa Pine ( $\times$ ), Mixed Southern Hardwoods ( $*$ ), Southern Yellow Pine( $+$ ), and White Fir ( $\boxplus$ ).

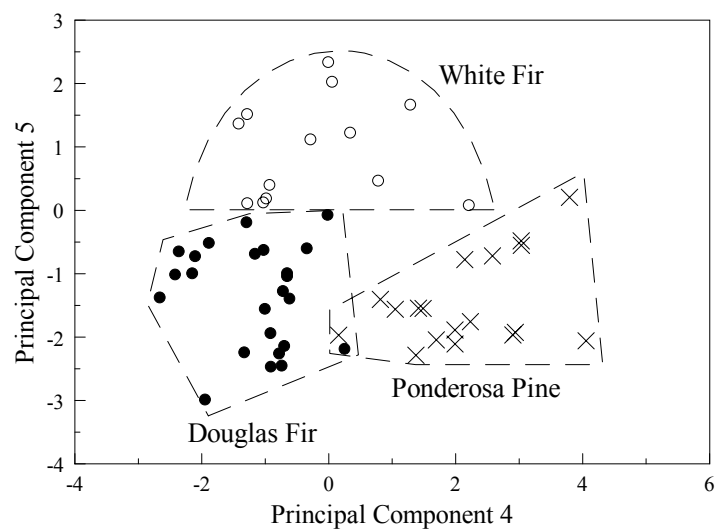


Figure 21. Plot of PLS principal components 5 versus 4, showing differentiation between white fir, Douglas fir, and ponderosa pine.

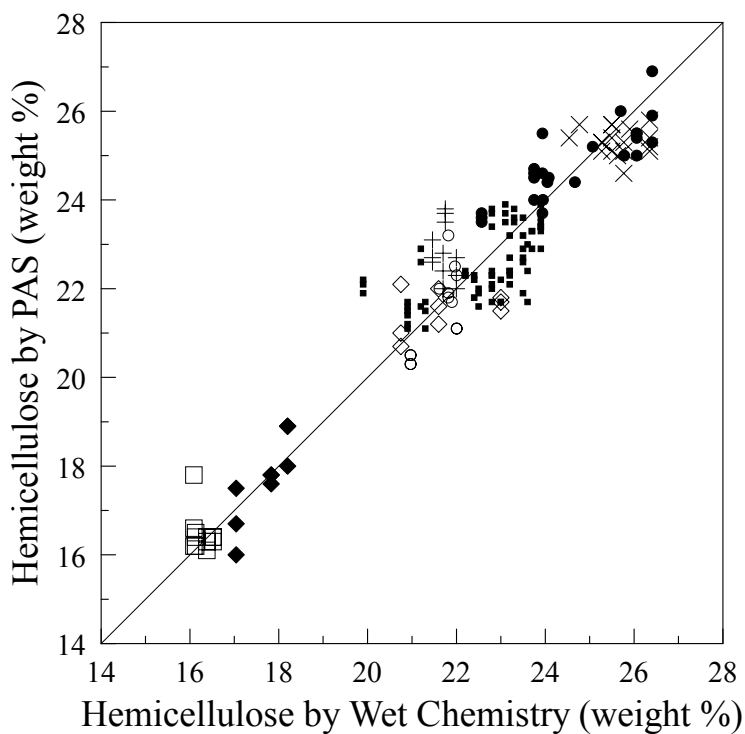


Figure 22. Quantitative analysis by PLS of hemicellulose for multiple samples of eight tree species. The standard error of prediction is 0.81 wt%. See the caption of Figure 20 for the tree species symbols.

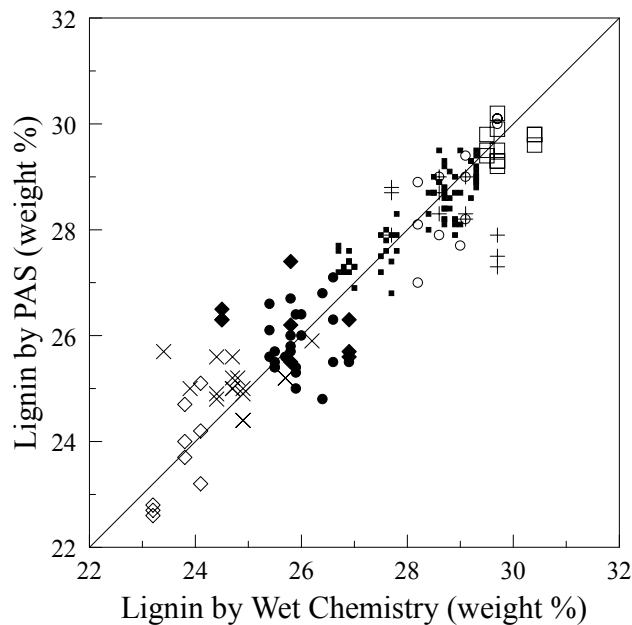


Figure 23. Quantitative analysis by PLS of lignin for multiple samples of eight tree species. The standard error of prediction is 0.70% wt. See the caption of Figure 20 for the tree species symbols.

### Application 3.

High surface specificity is required in FT-IR PAS measurements to characterize low concentrations of surface-treatment species on irregular surfaces such as fibers. Linearization of spectra, as described in the second section, achieves the highest surface sensitivity in FT-IR PAS measurements. Linearized and normal nonlinearized spectra of two fiber samples are shown in Figure 24, which were measured at 40 kHz scanning velocity. The absorption band at  $667\text{ cm}^{-1}$  is due to the chemical surface treatment, whereas the band at  $632\text{ cm}^{-1}$  is due to the fiber substrate. All of the spectra are scaled to a constant peak height of the  $632\text{ cm}^{-1}$  band. The linearized spectra show an increase in the intensity of the  $667\text{ cm}^{-1}$  surface species band by approximately a factor of three in both cases. The  $632\text{ cm}^{-1}$  band, which can be used as an internal reference, is not readily observable in ATR spectra of these samples, making it difficult to plot ATR spectra on a common scale. The adjustable sampling depth of PAS is useful in cases like this where simultaneous observation of a substrate band as an internal standard is useful.

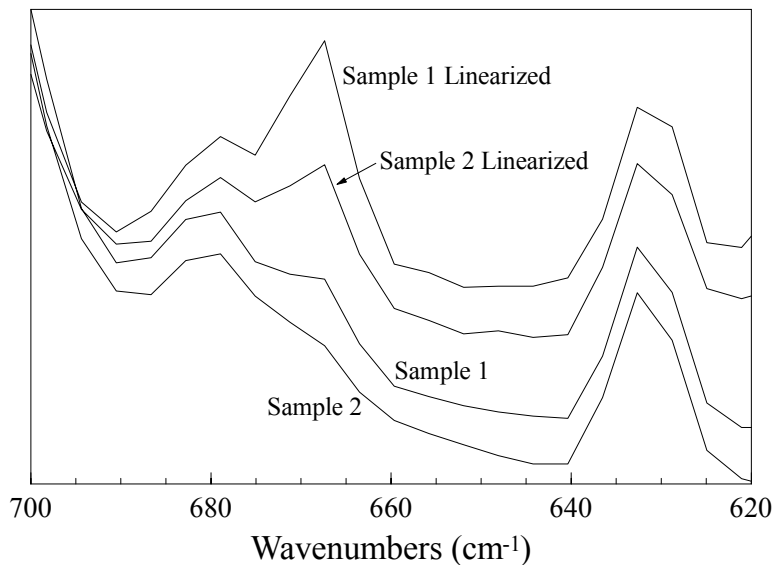


Figure 24. Photoacoustic spectra of fibers with different levels of surface treatment plotted as linearized and normal nonlinearized spectra. The treatment absorbance band is at  $667\text{ cm}^{-1}$ . Spectra have been scaled to the  $632\text{ cm}^{-1}$  substrate band.

#### Application 4.

This application's sample, consisting of a  $6\text{-}\mu\text{m}$  PET layer on a polycarbonate substrate, was discussed in the second section (see Figure 7) regarding the picking of a spectrum of a layer at a specific phase angle to best minimize features of other layers. Figures 25 and 26 show more of the magnitude and phase data on this sample. The normalized spectra of Figure 25 are calculated from  $S(\tilde{\nu},\phi)$  as given in equation (20). The top panel shows all of the spectra in the fingerprint region over a range of  $180^\circ$ . The data repeat after  $180^\circ$ . The spectra shown at  $\phi = 36^\circ$  and  $\phi = 75^\circ$  in Figure 7 are from this plot. The lower panel of Figure 25 shows the behavior of band peaks as a function of  $\phi$  in the manner of Figure 8. These plots are also from the upper panel of Figure 25, appearing if one looks from the phase angle axis. The PET peaks all reach a minimum before  $60^\circ$  and the polycarbonate peaks all have a minimum after  $60^\circ$ . The lower panel shows large and small bands from each layer exemplifying this behavior. The minima points of each set are within  $45^\circ$  of each other and all of the points of this two-layer system are within  $90^\circ$  of each other in accordance with the discussion in the second section.

Figure 26 shows the normalized magnitude and phase spectra calculated from  $S(\tilde{\nu})/S_b(\tilde{\nu})$  using equation (14), where  $S(\tilde{\nu})$  and  $S_b(\tilde{\nu})$  pertain to the sample and reference

spectra, respectively, and from  $\theta(\tilde{\nu})$  of equation (15). Note that the phase of the absorption bands of the pure polycarbonate spectrum all point to lower (faster) phase angles and are within a  $45^\circ$  range as predicted by the simple signal generation model for a homogeneous sample. The phase spectrum of the 6- $\mu\text{m}$  PET layer on polycarbonate sample, however, is much different because it is no longer homogeneous. The phase range now exceeds a range of  $45^\circ$  and only PET bands point to smaller phase angles, whereas the polycarbonate bands point to larger phase angles, which are indicative of PET being on top of polycarbonate rather than the opposite.

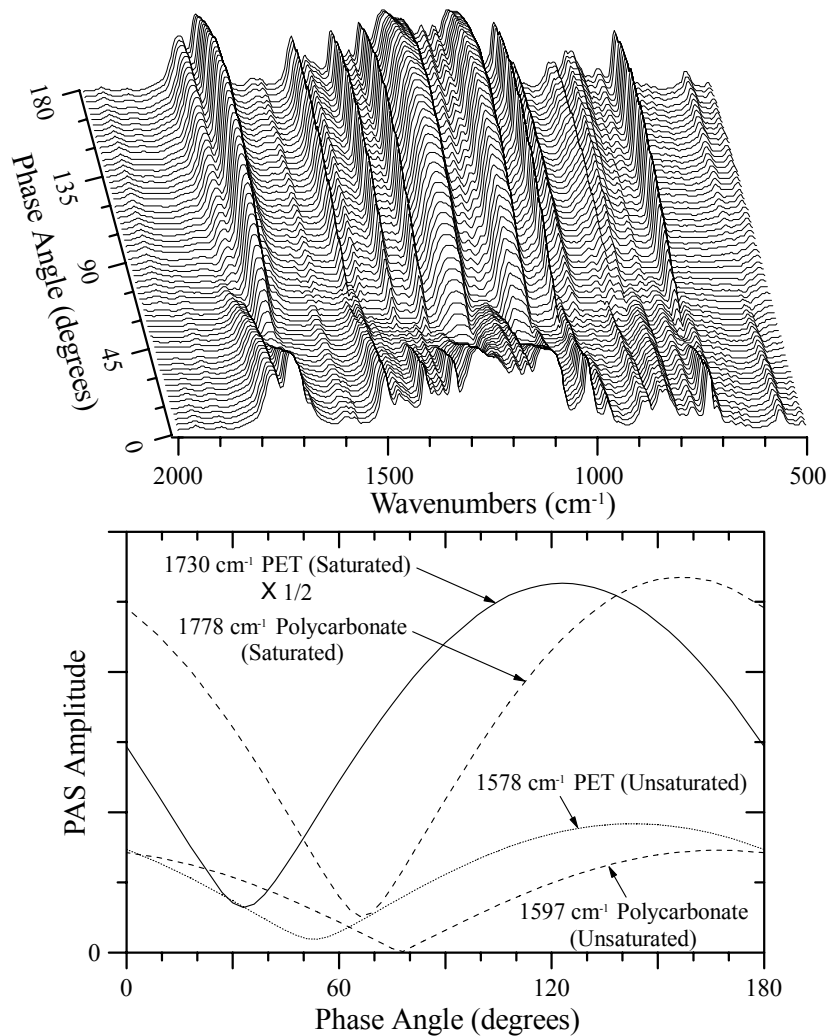


Figure 25. Three-dimensional (top panel) and peak amplitude versus phase angle (lower panel) presentations of data on a 6- $\mu\text{m}$  PET film on a polycarbonate substrate. The phase-scale zero is arbitrary.

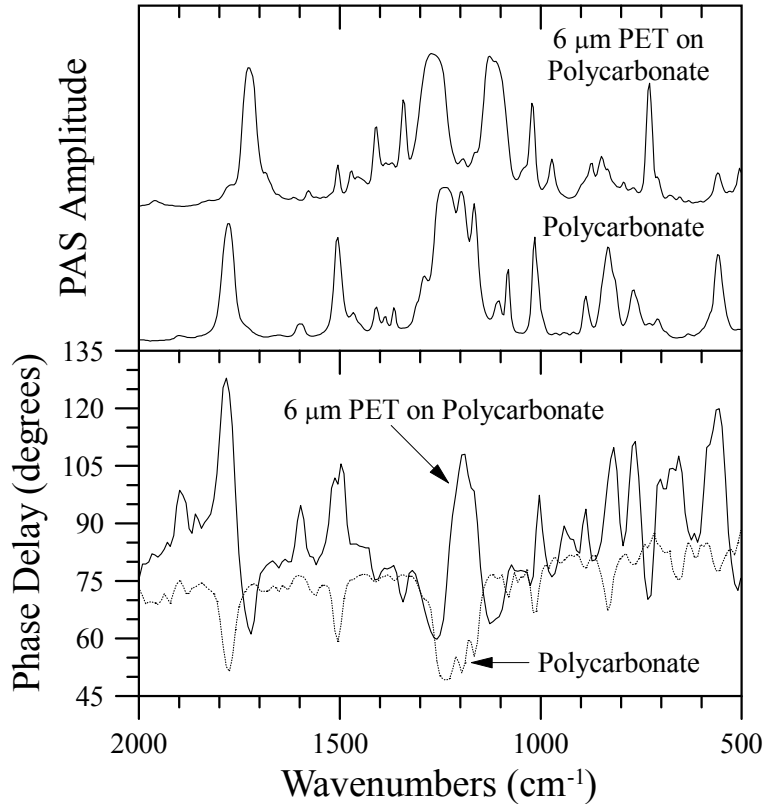


Figure 26. Amplitude and phase spectra measured with a rapid-scanning FT-IR spectrometer (laser frequency 20kHz) of polycarbonate with and without a 6- $\mu\text{m}$ -thick PET layer. The phase of the pure polycarbonate shows the expected behavior for a homogeneous sample, whereas the PET layer introduces the typical features of a nonhomogeneous sample. The phase scale zero is arbitrary.

#### Application 5.

This application involves analysis of a single fiber microsample which consists of a PET fiber coated with a thin layer of nylon. Figure 27 shows the magnitude spectra and phase behavior for selected band peaks measured at 400 Hz phase modulation frequency and  $8\text{ cm}^{-1}$  resolution. Note that the fiber spectrum bands picked for analysis are all of similar amplitude, so they would be expected to have roughly the same phase if the sample was homogeneous. Instead, the nylon bands are grouped together about  $15^\circ$  ahead of the PET bands. This indicates that the nylon is a coating on a PET core with a thickness of approximately  $2.4\text{ }\mu\text{m}$  using the value of  $0.16\text{ }\mu\text{m/degree}$  at 400 Hz from Table 2. It should be noted, however, that this thickness value may be distorted to some extent because the fiber geometry does not conform either optically or thermally to the planar geometry or to the one-dimensional optical and thermal propagation assumptions of the simple signal generation model.



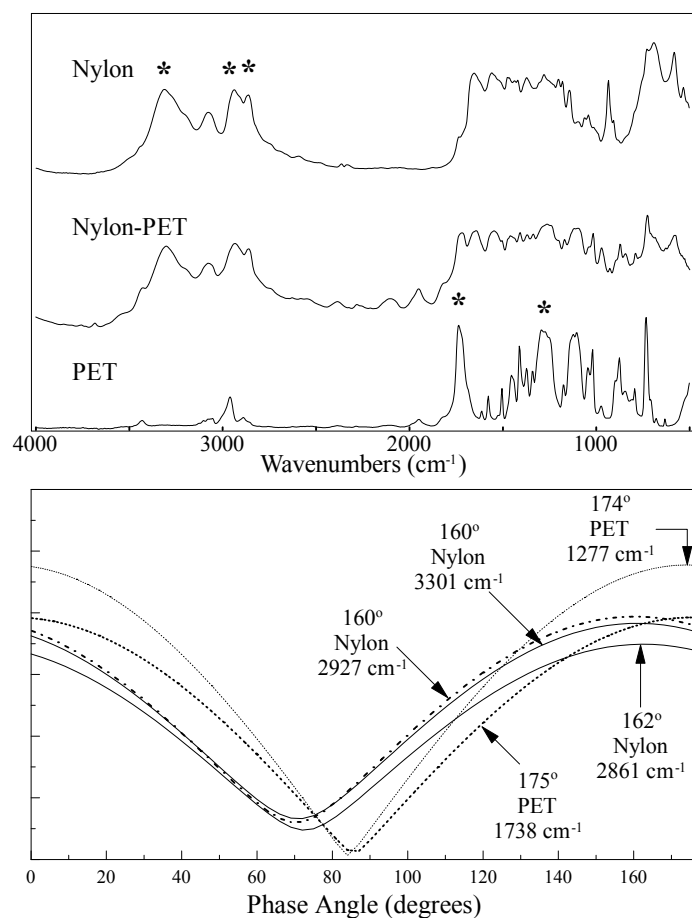


Figure 27. Amplitude versus wavenumber and phase angle of a single nylon-coated PET fiber. The phase angles of the nylon peaks are grouped approximately 15° from the grouped phase angles of PET. The phase scale zero is arbitrary.

#### Application 6.

This application demonstrates the capability of FT-IR PAS to resolve layer information on a dimensional scale that would not be practical using a sectioning and IR microscopy approach. The sample consists of two thin layers of different inks on a polyethylene substrate. The spectra of the inks on polyethylene, both individually and layered together, are shown in the top panel of Figure 28 and were measured at a phase modulation frequency of 400 Hz at 8 cm<sup>-1</sup> resolution. The bands representing each layer at 1467 cm<sup>-1</sup> (polyethylene), 1639 cm<sup>-1</sup> (blue ink), and 1782 cm<sup>-1</sup> (orange ink) were chosen in each case to be in spectral regions that were as free as possible of absorption from the other layers. Based on the relative amplitudes of these bands in the amplitude spectrum of the layered sample, the ordering of the phase minima of these peaks would be 1467 cm<sup>-1</sup>, 1639 cm<sup>-1</sup>, and 1782 cm<sup>-1</sup>, going from smaller to larger phase shifts if the sample were homogeneous. The ordering is actually the reverse, indicating that the

sample is not homogeneous and that the orange ink comprises the top layer, followed by the blue ink layer and then the polyethylene substrate. The orange-to-blue phase difference is  $5^\circ$  and the blue-to-polyethylene is  $18^\circ$  which indicates an orange layer thickness of  $0.8 \mu\text{m}$  and a blue layer thickness of  $2.9 \mu\text{m}$  assuming that the thermal diffusivity is close to  $10^{-3} \text{cm}^2/\text{s}$  for all layers and that the weaker absorption strengths of the  $1639 \text{cm}^{-1}$  and  $1782 \text{cm}^{-1}$  bands do not degrade the sharpness of boundary definition too much.

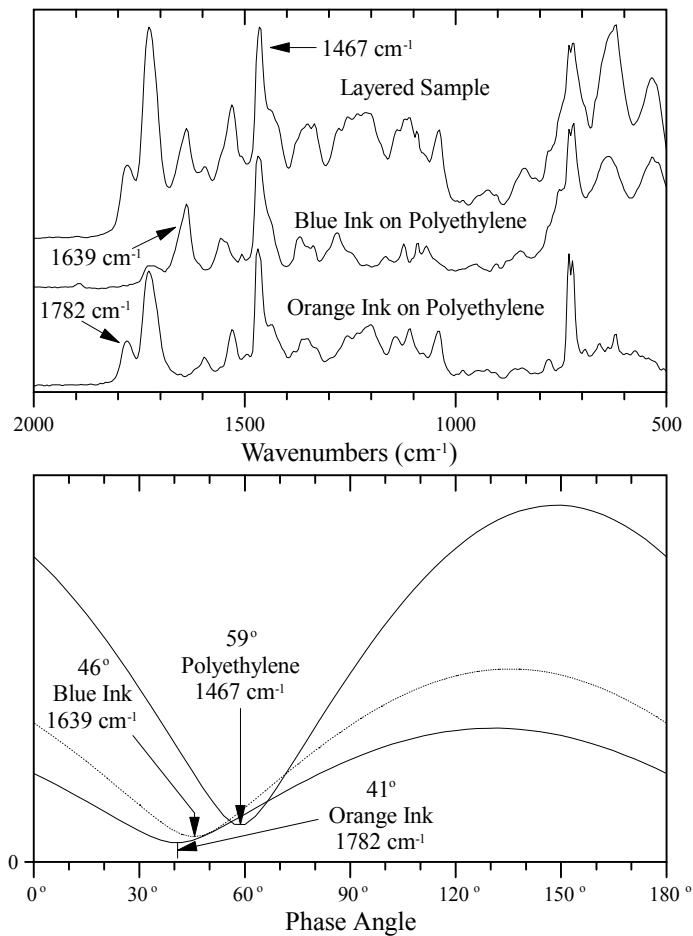


Figure 28. Amplitude versus wavenumber and phase angle for a layered sample with two very thin (less than approximately  $5 \mu\text{m}$ ) ink layers. The order of the layers is clearly defined from the data plotted in the lower panel as orange ink/blue ink/polyethylene. The phase scale zero is arbitrary.

## **Conclusion**

FT-IR PAS methods offer unique capabilities that allow analysis of a very wide range of sample types in the near- and mid-IR spectral regions. Samples with either homogeneous or depth varying compositions can be analyzed, in the latter case with higher depth resolution and depth range than is available by other IR sampling techniques. As recent and future advances in instrumentation and data analysis are put into wider use, FT-IR PAS is expected to play an increasingly important role in molecular spectroscopy particularly with layered and gradient materials.

## **Acknowledgements**

The authors thank Andreas Mandelis for providing the theoretical equations used to calculate the data in Figure 18, David Drapcho for information on impulse PAS, and Robert Meglen for the wood samples and chemometric results shown in Figures 20-23. This work was supported by MTEC Photoacoustics, Inc., Bio-Rad Laboratories, and the Ames Laboratory, which is operated for the USDOE by Iowa State University under contract No. W-7405-ENG-82.

## **Abbreviations and Acronyms**

DSP	Digital Signal Processing
LED	Light Emitting Diode
OPD	Optical Path Difference
PET	Poly(ethylene terephthalate)
PMMA	Poly(methyl methacrylate)
TIRS	Transient Infrared Spectroscopy
TRS	Time-resolved Spectroscopy

## References

1. D.W. Vidrine, 'Photoacoustic Fourier Transform Infrared Spectroscopy of Solids and Liquids' in "Fourier Transform Infrared Spectroscopy, Volume 3", J. R. Ferraro and L. J. Basile (Eds.), Academic Press, New York, Chapter 4, pp. 125-148 (1982).
2. J.F. McClelland, R.W. Jones, S. Luo, and L.M. Seaverson, 'A Practical Guide to FT-IR Photoacoustic Spectroscopy' in "Practical Sampling Techniques for Infrared Analysis", P.B. Coleman (Ed.), CRC Press, Boca Raton, FL, Chapter 5, pp. 107-144 (1993).
3. J.F. McClelland, S.J. Bajic, R.W. Jones, and L.M. Seaverson, 'Photoacoustic Spectroscopy' in "Modern Techniques in Applied Molecular Spectroscopy", F.M. Mirabella (Ed.) Wiley, New York, Chapter 6, pp. 221-265 (1998).
4. A.G. Bell, *Phil. Mag.*, **11**, 510-528 (1881).
5. A. Rosencwaig and A. Gersho, *J. Appl. Phys.*, **47**, 64-69 (1976).
6. F.A. McDonald and G.C. Wetsel, Jr., *J. Appl. Phys.*, **49**, 2313-2322 (1978).
7. H.S. Carslaw and J.C. Jaeger, *Conduction of Heat in Solids*, Clarendon, Oxford (1959).
8. L. Burggraf and D.E. Leyden, *Anal. Chem.*, **53**, 759-762 (1981).
9. J.F. McClelland, *Anal. Chem.*, **55**, 89A-105A (1983).
10. R.O. Carter III, *Appl. Spectrosc.*, **46**, 219-224 (1992).
11. R.W. Jones and J.F. McClelland, *Appl. Spectrosc.*, **50**, 1258-1263 (1996).
12. A. Mandelis, Y.C. Teng, and B.S.H. Royce, *J. Appl. Phys.*, **50**, 7138-7146 (1979).
13. E.Y. Jiang, R.A. Palmer, and J.L. Chao, *J. Appl. Phys.*, **78**, 460-469 (1995).
14. S.J. Bajic, R.W. Jones, and J.F. McClelland, to be submitted for publication.

15. [www.mtecpas.com](http://www.mtecpas.com)
16. R.A. Palmer, J.L. Chao, R.M. Dittmar, V.G. Gregoriou, and S.E. Plunkett, *Appl. Spectrosc.*, **47**, 1297-1310 (1993).
17. V.G. Gregoriou, M. Daun, M.W. Schauer, J. L. Chao, and R.A. Palmer, *Appl. Spectrosc.*, **47**, 1311-1316 (1993).
18. B.O. Budevskaja and C.J. Manning, *Appl. Spectrosc.*, **50**, 939-947 (1996).
19. R. Curbelo, U.S. Patent No. 5835213 (1998).